Published in : Methods (2018), vol. 144, pp. 125–133
DOI: 10.1016/j.ymeth.2018.03.010
Status : Postprint (Author's version)

PREDICTING ION MOBILITY-MASS SPECTROMETRY TRENDS OF POLYMERS USING THE CONCEPT OF APPARENT DENSITIES

Jean R.N. Haler[a,*], Denis Morsa[a], Philippe Lecomte[b], Christine Jérôme[b], Johann Far[a], Edwin De Pauw[a]

[a]*Mass Spectrometry Laboratory, University of Liège, MolSys Research Unit, Quartier Agora, Allée du Six Aout 11, B-4000 Liège, Belgium*

[b]*Center for Education and Research on Macromolecules, University of Liège, CESAM Research Unit, Quartier Agora, Allée du Six Aout 13, B-4000 Liège, Belgium*

**Corresponding author : J.R.N. Haler*

Keywords:

Ion Mobility-Mass Spectrometry, Synthetic polymers, Gas phase structures, Apparent densities, Data fitting, Prediction

Abstract

Ion Mobility (IM) coupled to Mass Spectrometry (MS) has been used for several decades, bringing a fast separation dimension to the MS detection. IM-MS is a convenient tool for structural elucidation. The folding of macromolecules is often assessed with the support of computational chemistry. However, this strategy is strongly dependent on computational initial guesses. Here, we propose the analysis of the Collision Cross-Section (CCS) trends of synthetic homopolymers based on a fitting method which does not rely on computational chemistry *a prioris* of the three-dimensional structures. The CCS trends were evaluated as a function of the polymer chain length and the charge state. This method is also applicable to mobility trends. It leads to two parameters containing all information available through IM(-MS) measurements. One parameter can be interpreted as an *apparent density*. The second parameter is related to the shape of the ions and leads us to introduce the concept of trends *with constant apparent density*. Based on the two fitting parameters, a method for IM trend predictions is elaborated. Experimental deviations from the predictions facilitate detecting structural rearrangements and three-dimensional structure differences of the cationized polymer ions. This leads for instance to an easy identification and prediction of the presence of different polymer topologies in complex polymer mixtures. The classification of predicted trends could as well allow for software-assisted data processing. Finally, we suggest the link between the CCS trends of homopolymers and those obtained from (monodisperse) biomolecules to interpret potential folding differences during IM-MS studies.

Published in : Methods (2018), vol. 144, pp. 125–133
DOI: 10.1016/j.ymeth.2018.03.010
Status : Postprint (Author's version)

1. Introduction

Ion Mobility-Mass Spectrometry (IM-MS) is a gas phase technique used to separate ions having different Collision Cross-Sections (CCSs); a quantity that is correlated to their three-dimensional structures. IM-MS studies on polymers have been undertaken for several decades with special focus on computational chemistry support for structural interpretations of the observed pseudo-molecular species in the gas phase [1–9]. However, the polymers' potential to build a general model to correlate the CCS trends as a function of the mass [10–14] to a model structure has not yet been systematically explored.

Contrary to the usual monodispersity of biopolymers, polydisperse synthetic polymer samples provide a wide mass range of identical compounds (i.e., polymer chain length distribution). They are observed at several charge states during a single Electrospray Mass Spectrometry (ESI MS) experiment. The polymer ions' Arrival Time Distributions (ATDs) acquired by Ion Mobility (IM) then lead to a widely distributed CCS range. Evolutions of the CCS of growing polymer chains can therefore be monitored at different charge states and for large data sets in which intramolecular interactions are of constant nature. From an experimental point of view, each polymer ion of a given synthetic polymer can usually be associated to a unique CCS value per charge state and per polymer length [4,8,9,15], further enabling the monitoring of CCS evolutions. However, multiple CCS values or evolutions associated to given polymer-cation complexes were sometimes observed [16,17]. They were in most cases traced back to multimer formation and lacking mass spectrometric resolving power [18,19].

The observation of unique ATD peaks for each polymer-cation complex simplified the study of the CCS evolutions of different polymer topologies, such as linear, cyclic [20] and several star topologies [4,21] of poly(caprolactone) (PCL) and poly(lactide) (PLA) [22]. Different topologies of polydisperse PCLs were used to demonstrate that, dependent on the topology, the CCS did not rise identically with the mass (or degree of polymerization). Conformational analyses have been undertaken on poly(ethylene glycol) PEG [15] and PLA [7] using IM-MS or ion mobility spectrometry supported by Molecular Dynamics (MD) simulations. Structural transitions between globular and elongated '*beads on a string*' conformations were highlighted by computational chemistry [8,9]. Globular shapes of these polymers were exhibited for the explored charge states provided that the polymer chain lengths were sufficient for efficient solvation of the complexed alkali cations. On the contrary, '*beads on a string*' conformations emerged for highly charged, small polymer chain lengths [4,7–9,15].

The computed three-dimensional structures presented in the above-mentioned articles [1,2,4,7–9] were deduced from the CCS data, a two-dimensional information (related, to a certain extent, to a surface area) obtained from Ion Mobility. These Molecular Dynamics or Molecular Mechanics (MM) simulations yield several potential candidate structures having computed CCSs compatible with the experimental IM values. The computational methods often differ in the used force fields, simulation lengths or annealing methodologies, and even in the parameters or algorithms used for CCS predictions (e.g. using mobcal [23,24], IMoS [25,26], projection approximation, exact hard sphere scattering, trajectory method), but no exact match between these predicted and experimental CCS

Published in : Methods (2018), vol. 144, pp. 125–133
DOI: 10.1016/j.ymeth.2018.03.010
Status : Postprint (Author's version)

values was usually found. Moreover, the modeling of ion-particle interactions is not yet fully understood and their descriptions are still being refined [25].

Here, we investigate the CCS evolutions of five mass-dispersed synthetic homopolymers as a function of the mass and the charge using solely experimental ESI IM-MS measurements, distancing ourselves from computational chemistry *a prioris* on the three-dimensional structures. First, a CCS data fitting method is proposed which leads us to discuss the experimental IM structures of polymers in the gas phase. From the CCS fit trends, we introduce the concept of *trends with constant apparent densities*. From this model, a prediction method of CCS evolutions is elaborated and the applications of the methodology are discussed. The fitting method is extended from CCS data to drift time and mobility data. We also propose the use of the homopolymers' CCS trends to assist the interpretation of the folding variations of biopolymers and biomolecules based on IM-MS approaches.

2. Materials and methods

2.1. CHEMICALS

A detailed list of the chemicals used can be found in the **Supplementary information**.

2.2 POLYMERS

The syntheses of poly(caprolactone) PCL star topology polymers were described by Morsa and coworkers [4]. Poly(ethylene oxide) PEO (CH_3O-PEO-H) 5000 g/mol was bought from Aldrich. Following the synthesis of the monomer (see **Supplementary information**), poly(ethoxyphosphate) (poly(2-ethoxy-1,3,2-dioxaphospholane 2-oxide)) PEtP polymers [27] (1200 g/mol, 3000 g/mol, 4500 g/mol, 5500 g/mol; **Fig. SI1**) were synthesized as described in the Supplementary information.

2.3 ELECTROSPRAY IONIZATION IN POSITIVE MODE COUPLED TO ION MOBILITYMASS SPECTROMETRY

Poly(ethylene oxide) and poly(ethoxyphosphate) polymers were solubilized in pure methanol spiked with Na^+ cations (NaCl salt) to yield concentrations of polymer complexes ranging from 2×10^{-6} M to 10^{-5} M, depending on the sample. Poly(ethoxyphosphate) polymers were cationized as well using Ca^{2+} cations ($CaCl_2 \cdot 2H_2O$ salt) to yield concentrations of polymer complexes on the order of 5×10^{-6} M. For detailed information on the SYNAPT G2 HDMS traveling wave Ion Mobility-Mass Spectrometer (Waters, Manchester, UK) experimental parameters see the **Supplementary information**.

Sample preparation and ESI conditions for poly(caprolactone) polymers were described elsewhere [4]. A SYNAPT G1 Ion Mobility-Mass Spectrometer (Waters, Manchester, UK) was used to determine the ATDs of PCLs.

The interpretation of the 2D data (drift time as a function of the mass-to-charge ratio) was performed using Waters MassLynx 4.1 and Driftscope 2.1 software. ATD peaks were fitted (Gaussian function)

Published in : Methods (2018), vol. 144, pp. 125–133
DOI: 10.1016/j.ymeth.2018.03.010
Status : Postprint (Author's version)

using PeakFit v.4.11 to accurately define the apex of each ATD peak. Data processing was performed using Excel 2011, SigmaPlot 12.0 and IgorPro 6.34A.

2.4. COLLISION CROSS-SECTION/ION MOBILITY CALIBRATION

For the full details of the calibration process [28] see the **Supplementary information**. IM data were acquired using a traveling wave IM-MS operated in N_2 as drift gas and the CCS calibrations were performed using reference substances acquired in drift tube IM operated using He as drift gas [18,29–33] (He-derived T-Wave$_{N2}$ CCS).

2.5. FITTING THE CCS EVOLUTIONS

The CCS evolution fitting is an iterative process, where one has to evaluate the quality of the fit going through the data points. The data points for the fits are constituted by all the points between the structural rearrangements (tipping points). Once a fit is performed on several data points, one can (re-)evaluate whether it takes correctly account of the chosen data points or if more/fewer points should be included. The structural rearrangements then also become more clearly visible and the data point choices become more apparent.

3. Results and discussion

The Mason-Schamp equation [34] provided in **Eq. (1)** links the mobility of an ion *K* to its charge *z*, the reduced mass of the ion and the drift gas μ and the rotationally-averaged Collision CrossSection (converted to Å^2). The average CCS (X_{avg}) being related to the ion mobility K, the CCS usually increases with the polymer chain length due to the higher mass (and related size) of the polymer.

$$\mathrm{K} = \frac{3}{16}\frac{e}{N}\left[\frac{2\pi}{\mu k_B T}\right]^{\frac{1}{2}}\frac{z}{\Omega_{avg}} \qquad \textbf{(1)}$$

where *e* is the elementary charge, k_B is the Boltzmann constant, *T* is the temperature and *N* is the gas number density.

Using a traveling wave ion guide instrument usually requires a calibration procedure to convert the ATDs into CCS values for each set of experimental settings (see Materials and Methods section). The *m*/*z* ratios corresponding to polymer-cation complexes were converted into DP values (Degree of Polymerization), i.e., providing the number of polymerized monomer units associated with an identified charge state. This process is similar to the one used in the Kendrick mass scale [35]. The *m*/*z* to DP conversion enables the comparison of CCS trends of different charge states from polymers being constituted of monomer units having different masses.

3.1. TREND LINES AND COMMON TREND LINE

Fig. 1 shows the plot of the CCS evolution as a function of the DP of linear poly(ethoxyphosphate) PEtP topology at various charge states. For a given charge state, the CCS is steadily and monotonically

Published in : Methods (2018), vol. 144, pp. 125–133
DOI: 10.1016/j.ymeth.2018.03.010
Status : Postprint (Author's version)

increasing with increasing DP values, similarly to various polymer-cation complexes described in literature [3,4,7–9,15,19,2 1,22,36–38].

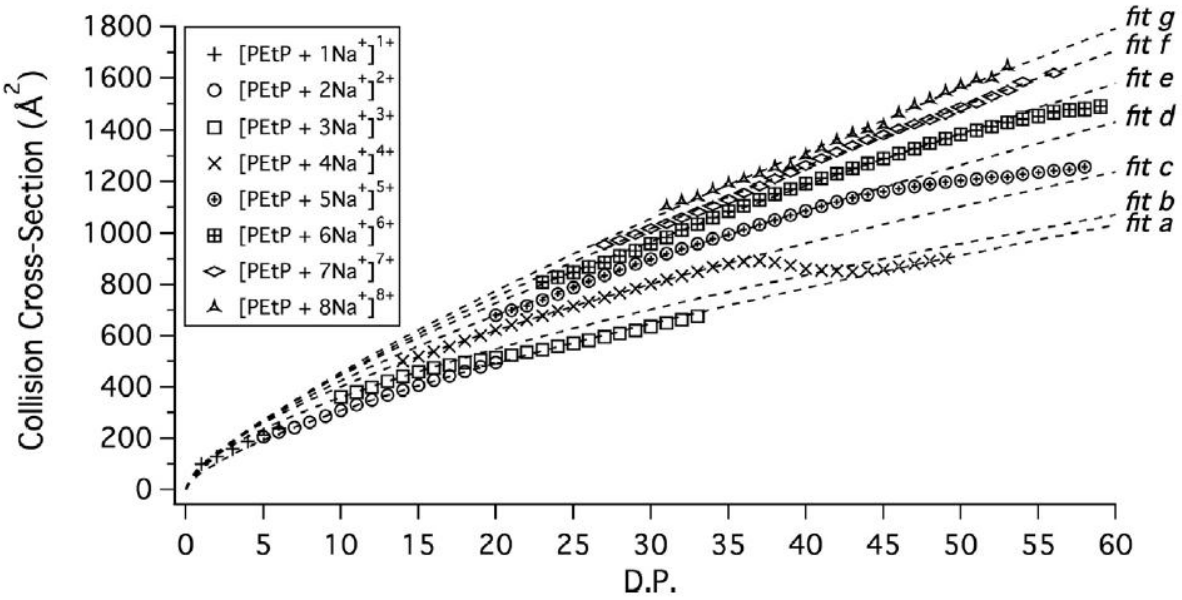

Fig. 1. Plot of the Collision Cross-Section (CCS, He-derived-T-Wave$_{N2}$ CCS) versus the DP (Degree of Polymerization) of sodiated poly(ethoxyphosphate) (PEtP) polymer ions at different charge states (1+ to 8+). The plot shows unconstrained power fit functions (*CCS = A.DP^{pow},* **Eq. (2)**) for the different CCS trends before and after the tipping points (described as *fit a* to *fit g*). **Fig. SI12** highlights the data points used for performing the data fits.

Nonetheless the CCS evolutions of some charge states (i.e., >1+) of polymers show tipping points that do not follow their initial monotonically increasing CCS evolution. These tipping points lead to higher DPs not acquiring larger CCS values than the previous DPs. Interestingly, the CCSs from these tipping points eventually reach the CCS evolution built by a lower charge state. The CCS evolutions and the tipping points originate from the balance between enthalpic and entropic contributions of the growing polymer chain and the Coulomb repulsion of the cation charges. Ultimately, as for PEtP bearing 3 or 4 charges, the CCSs from the tipping points reach the CCS evolution established by the lowest possible polymer ion charge state, i.e., the singly charged polymer, as shown in **Fig. 1**. This CCS evolution of singly charged ions represents the most compact polymer ion structure [37].

When fitting the CCS evolutions as a function of the DP before and after the tipping points, we found that they were best described by a power law fit function, as described in **Eq. (2)**. This provides different (CCS) trends according to the DP and the charge state. We propose to denote the trend of the most compact polymer ions as the *common trend line* [17] because all the higher charge state trends will eventually follow this trend line at high enough DP values [9,15].

$$\Omega = A \cdot DP^{pow} \qquad \textbf{(2)}$$

where Ω is the rotationally-averaged Collision Cross-Section, DP is the Degree of Polymerization of the polymer (number of monomer units) and *A* and *pow* are fit parameters.

Published in : Methods (2018), vol. 144, pp. 125–133
DOI: 10.1016/j.ymeth.2018.03.010
Status : Postprint (Author's version)

3.2. POWER LAW FITS FOR SPHERICALLY-SHAPED IONS

The common trend line has been associated in literature [4,7– 9,15,17,37] with spherical ion shapes. Indeed, the common trend line contains the CCS trend of the 1+ charge state where no Coulomb repulsion distorts the ion shape. Aside from the 1+ charge state, the CCS trends of the 2+ charge state as well as contributions at high DPs from the 3+ and 4+ charge states after their tipping points make up the common trend line of PEtP. Empirical fitting of the CCS evolution was performed using **Eq. (2)** ('fit a' in **Fig. 1**). The trend fits with the spherical shape trend as pow approaches 2/3 (0.66) [28].

Fig. 2 depicts the CCSs of poly(ethylene oxide) PEO complexed with 3–9 Na^+ cations as a function of the DP, ranging from around 90 to around 145. The CCS evolution of PEO complexes bearing 3 cations at the DPs above 100 correlates with the common trend line [9,15]. Our results of the PEO common trend line fit are in good agreement with the spherical shape trend or an isotropic shape growth (i.e., *pow = 0.66*; '*fit a*' in **Fig. 2**). Like PEtP-sodium complexes, higher charge states of PEO ions exhibit tipping points and CCS trends merging with more compact CCS trends.

Eq. (2) for spherical shapes (*pow = 0.66*, **Eq. (7)**) can be retraced through the development of **Eq. (3)** to **Eq. (6)** (similar to [36]) where the volume of a sphere (**Eq. (3)**) can be reformulated in the case of homopolymers (**Eq. (4)**). The CCS represents a surface which can thus be approximated by **Eq. (5)** within the hypothesis of two non-interacting bodies as described by the hard sphere approximation model [39]. In this case, the ion-neutral contact distance is defined as the sum of the two radii. Nonetheless, considering that the ion radius of the polymer-alkali complexes is much greater than the buffer gas radius, the sum of the radii can be simplified to the polymer radius only (**Eq. (5)**). This simplification can easily be performed for high DP polymer chains and stands as an approximation for very small polymer chains. Finally, we can rewrite **Eq. (2)** and formulate the Collision Cross-Section as a function of the DP and a volume contribution of a polymerized monomer unit in the hard sphere approximation, as expressed by **Eq. (6)**. We will henceforth refer to 'polymerized monomer unit' as 'monomer (unit)'.

$$V_{sphere} = \frac{4}{3}\pi r^3 = V_{polymer} \qquad \textbf{(3)}$$

where V_{sphere} is the volume of a sphere, r is the radius of the corresponding sphere and $V_{polymer}$ is the total volume of the polymer.

$$V_{polymer} = DP \cdot V_{mono} \qquad \textbf{(4)}$$

where DP is the Degree of Polymerization of the polymer and V_{mono} is the mean volume of a polymerized monomer unit in the gas phase, i.e., a repetitive building block of the polymer.

$$\Omega = \pi\xi\left(r_{ion} + r_{gas}\right)^2 \cong \pi\xi r_{ion}^2 \qquad \textbf{(5)}$$

where Ω is the CCS, ξ is the momentum scattering coefficient [40] and r_{ion} and r_{gas} are the radii of the ion or the neutral drift gas particle, respectively. **Eq. (5)** assumes that $r_{ion} >> r_{gas}$.

$$\Omega = \left[\left(\frac{3}{4}\right)^{2/3} \pi^{1/3} \xi V_{mono}^{2/3}\right] \cdot DP^{2/3} \qquad \textbf{(6)}$$

Eq. (6) is equivalent to **Eq. (2)** where *pow = 2/3*. The parameter *A* describes the terms in brackets of **Eq. (6)**. It depends on the apparent volume of the monomers constituting the polymer in the gas phase.

Published in : Methods (2018), vol. 144, pp. 125–133
DOI: 10.1016/j.ymeth.2018.03.010
Status : Postprint (Author's version)

$$\Omega = A \cdot DP^{2/3} \qquad \textbf{(7)}$$

where Ω represents the CCS, *A* is the fit parameter and *DP* is the Degree of Polymerization.

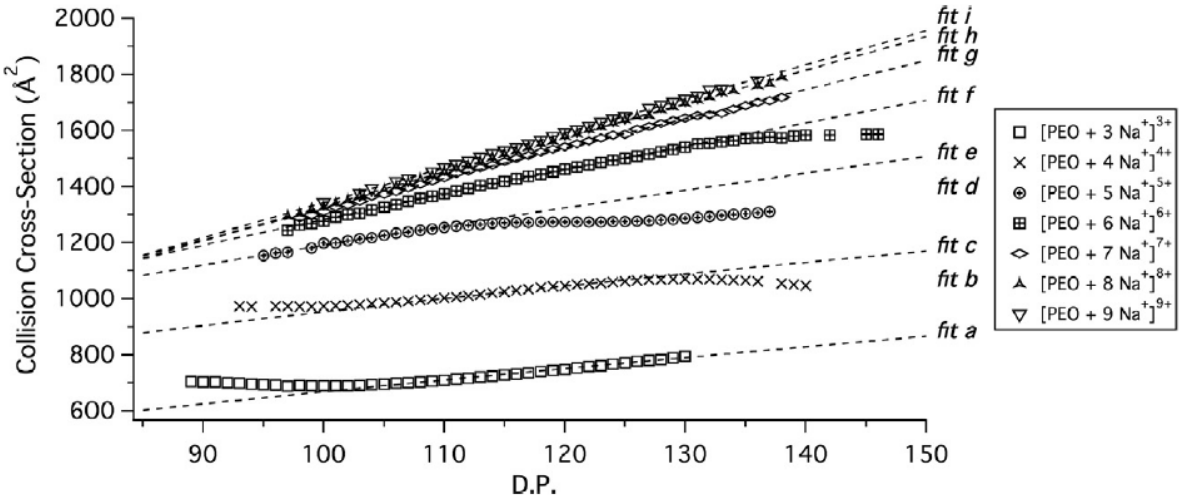

Fig. 2. Plot of the Collision Cross-Section (CCS, He-=derived-T-Wave$_{N2}$ CCS) as a function of the DP (Degree of Polymerization) of sodiated poly(ethylene oxide) (PEO) polymer ions at different charge states (from 3+ to 9+). The unconstrained power fit functions (*CCS = A.DP^{pow}*, **Eq. (2)**) for the different CCS trends before and after the tipping points are described as *fit a* to *fit i*. The fit functions *fit b* and *fit d* are not shown but are still accounted for in the plot as they denote the CCS trends missed in the analyzed DP range. **Fig. SI13** highlights the data points used for performing the data fits.

3.3. PHYSICAL MEANING OF THE FIT PARAMETER A

Eq. (6) coupled to the volumetric mass density of one monomer unit in the polymer leads to the concept of *an apparent density* in the gas phase (**Eq. (8)**) represented by the fit parameter A from **Eq. (2)** (or **Eq. (7)**).

$$A = \left(\frac{3}{4} \cdot \frac{MM_{mono}}{N_A} \cdot \frac{1}{d}\right)^{2/3} \pi^{1/3} \xi \qquad \textbf{(8)}$$

where *A* is the fit parameter from **Eq. (2) or (7)**, MM_{mono} is the molar mass of the monomer, *d* is the (volumetric mass) density reported to a monomer unit and N_A is the Avogadro number.

The parameter *A* bears empiric information specific to the chemical nature of the polymer and its interactions with the cationizing agents, here the solvated alkali cations. The parameter *A* embodies the added mean volume at the origin of the CCS increase when adding a monomer unit. This added monomer unit (mass increase) solvates an increment of the total ion charge in its mean volume. A larger parameter *A* value then translates into a lower apparent density. The apparent density thus reflected by the parameter *A*, together with its pow fit parameter (**Eq. (2)**), defines a CCS trend and classifies ions into 'trends with constant apparent density'. The value of the parameter A takes into account both the enthalpic (e.g., charge solvation by coordination and Coulomb repulsion between charges) and the entropic (favoring spherical shapes) contributions, which yield stable structures in the gas phase.

Published in : Methods (2018), vol. 144, pp. 125–133
DOI: 10.1016/j.ymeth.2018.03.010
Status : Postprint (Author's version)

To illustrate the influence of the chemical nature of the polymer on the fit parameter *A*, we can compare the fit parameters of the common trend lines of poly(ethoxyphosphate) PEtP ('*fit a*' in **Fig. 1** and **Table 1**) and poly(ethylene oxide) PEO ('*fit a*' in **Fig. 2** and **Table SI2**) cationized with Na^+. The *A* fitting parameters (**Eq. (2)**; ±95% confidence interval) for the common trend lines of PEtP and PEO are *65.1 ± 2.1* and *35.2 ± 4.1*, respectively.

Table 1
Fitting parameters of several trend lines for poly(ethoxyphosphate) PEtP. The fits ($CCS = A.DP^{pow}$) are calculated with free *A* and *pow* parameters.

Polymer	Fitting curve	Charge state description	*pow*[1]	*A*[1]
PEtP	*Fit a*	Common trend line (2+ to 4+)	0.67 ± 0.01	65.1 ± 2.1
	Fit b	3+	0.61 ± 0.04	88.4 ± 9.0
	Fit c	4+	0.63 ± 0.00	94.5 ± 1.4
	Fit d	5+	0.68 ± 0.01	88.9 ± 2.8

[1]The values of the *pow* and *A* fitting parameters are given with their 95% confidence interval.

3.4. OBSERVING POW∼0.66 FOR MULTIPLE CCS TRENDS AND TREND-SPECIFIC FIT PARAMETER A

Aside from the ions of the common trend line, any isotropically growing object, or any object subjected to free rotation and having no preferential orientation should lead to a CCS value of a hypothetical spherical object of equivalent uniform density. A CCS representing a surface, i.e., the two-dimensional surface defined by the interaction of the ion with the drift gas, can mathematically be expressed by a radius raised to the power of 2. Any three-dimensional structure has a volume proportional to a radius parameter raised to the power of 3. The *pow* parameter could hence as well be expressed by the ratio of these terms, i.e., *0.66* (*2/3*) for shapes other than true spheres. This leaves the structural differences to be described by changes in the apparent density parameter *A* (**Eq. (8)**). The equations and the development of the formulae (**Eqs. (3)-(8)**) would thus become independent of the starting hypothesis, i.e., spherical or near-spherical shapes. As the parameter *A* changes from one folding to another, one preferably should adopt the denomination of apparent spherical structures or '*trends with constant apparent density*' (**Eq. (8)**).

Literature postulates elongated shapes for polymer-alkali cation complexes at high charge states[4,7–9,15] but our fit for e.g., the 5+ charge state $[PEtP+5Na^+]^{5+}$ still provides a *pow* parameter approaching *2/3* (*0.68 ± 0.01*; **Fig. 1** '*fit d*'). This is in close agreement with *0.66* (or *2/3*) and with the *pow* parameters observed for the common trend lines of PEtP and PEO (*0.67 ± 0.01* and *0.64 ± 0.02*, respectively). Such *pow* values could suggest a globular shape of the ions (or regions of apparent isotropic growth), at least as perceived by ion mobility in the gas phase. In agreement with **Eq. (8)**, the IM-MS fit suggests that the shape associated with the CCS is of lower apparent density (*A = 88.9 ± 2.8*) for $[PEtP+5Na^+]^{5+}$ than the more compact shape of $[PEtP+1Na^+]^{1+}$ (*A = 65.1 ± 2.1*). The apparent density decreases when the charge state increases as the ion shapes 'bloat' due to Coulomb repulsions. Once the charge repulsion is more effectively screened by the addition of monomer units (i.e., increasing the DP), the ion apparent densities decrease until they eventually reach the maximum density defined by the common trend line. The fit parameter *A* value is hence specific from one fit (or trend) to another.

Published in : Methods (2018), vol. 144, pp. 125–133
DOI: 10.1016/j.ymeth.2018.03.010
Status : Postprint (Author's version)

3.5. TREND ANNOTATIONS: CONSTRAINING POW TO 0.66 AND CONSTANCY OF THE PARAMETER A RATIOS (0.9)

Now we constrain the *pow* parameter from **Eq. (2)** to *0.66* (*2/3*) during the development of the fitting methodology for polymer trend comparisons while the parameter *A* is kept unconstrained (**Eq. (7)**; see **Table 2** and **Fig. SI4** for PEtP). Any structural information yielded by IM-MS, depending on the chemical nature and the interactions of the monomers within the polymers, is then enclosed within the parameter *A*. At this stage, no conclusion on the shape of the ions (e.g., sphere or '*beads on a string*') will be drawn because the parameter *A* only reflects the apparent density of an assumed and hypothetical spherical structure (i.e., *pow = 2/3*) of equivalent apparent density. The information contained in the pow parameter is related to a shape factor and will be detailed in a future paper.

We can now evaluate the ratios of the parameter *A* values of any successive trends with constant apparent density. **Eq. (9)** can be established when combining **Eq. (7)** and **Eq. (8)**. The parameter *A* ratio is equivalent to the CCS ratio, which are related to the apparent density ratios of the polymer-cation complexes.

$$\frac{A_1}{A_2} = \frac{\Omega_1}{\Omega_2} \propto \left(\frac{d_2}{d_1}\right)^{2/3} \qquad \textbf{(9)}$$

Where A_1 and A_2 are the fitting parameters of two different trends with constant apparent density, (see **Eq. (2)** and **(7)**), Ω_1 and Ω_2 are CCS values and d_1 and d_2 are the (volumetric mass) densities reported to a monomer unit.

Table 2 shows the ratios of the parameters *A* for PEtP complexes of two identified successive trends with constant apparent density, i.e., A_n and $A_{(n+1)}$. When comparing their ratios, a recurring value of around 0.9 is found for alkali metal cationized ions. This value of 0.9 is observed as the general pattern when jumping from one trend with constant apparent density to the next. We hence observe a 10% decrease in apparent density (parameter *A*) when going from the structural trend '*n*' to the next trend '*n + 1*'. Interestingly, this is also valid for the other investigated polymers such as PEO (**Fig. 2** and **Fig. SI6**) and linear PCL (**Fig. 3**). They also provide the same parameter *A* ratio values of 0.9 (**Table 2**).

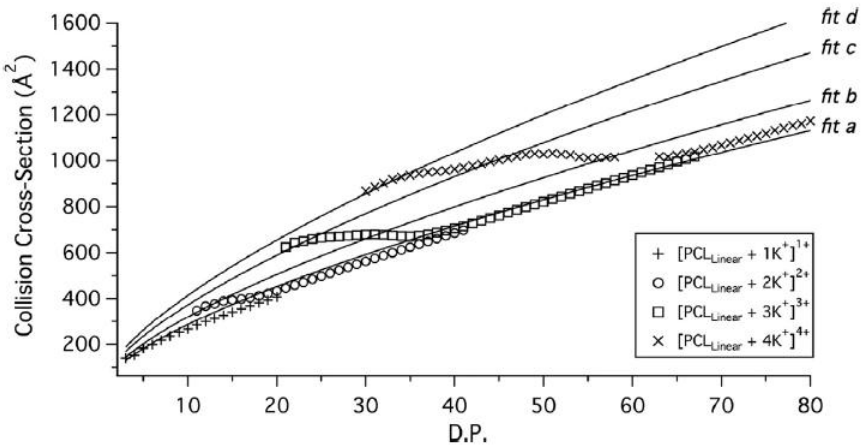

Fig. 3. Plot of the Collision Cross-Section (CCS, He-derived T-Wave$_{N2}$ CCS) versus the DP (Degree of Polymerization) of linear poly(caprolactone) (PCL) polymers with varying numbers of potassium cations used to reach different charge states (from 1+ to 4+). The constrained power fit functions (CCS = A.DP$^{0.66}$, Eq. (7)) for the different CCS trends before and after the tipping points are described as fit a to fit d. Fig. SI14 highlights the data points used for performing the data fits.

Published in : Methods (2018), vol. 144, pp. 125–133
DOI: 10.1016/j.ymeth.2018.03.010
Status : Postprint (Author's version)

Table 2

Fitting parameters of the trend lines for poly(ethoxyphosphate) PEtP (either sodium or calcium cationized), poly(ethylene oxide) PEO (sodium cationized) and different topologies of poly(caprolactone) PCL (potassium cationized) polymer-cation complexes. The constrained fits ($CCS = A.DP^{0.66}$, **Eq. (7)**) are calculated with free *A* but constrained *pow* parameters. Fitting parameter *A* ratios, representing the ratios of the densities of the different apparent spherical trends, are provided as well.

Polymer	Fitting Curve	Charge State Description	A[1]	$A_{Trend\ n}/A_{Trend\ (n+1)}$	$A_{CommonTrendline}/A_{Trend3+}$
PEtP[2]	*Fit a*	Common trend line (2+ to 4+)	68.6 ± 0.3	0.89	
(Na^+)	*Fit b*	3+	77.4 ± 0.9	0.91	
	Fit c	4+	85.3 ± 0.3	0.90	
	Fit d	5+	95.0 ± 0.2	0.92	
	Fit e	6+	103.8 ± 0.5	0.94	
	Fit f	7+	110.8[4] ± 0.8	0.96	
	Fit g	8+	115.9[4] ± 0.9		
PEtP[6]	*Fit a*	Common trend line (2+ and 4+)	68.1 ± 0.2	0.83	
(Ca^{2+})	*Fit c*	4+	82.0 ± 0.5		
PEO[2]	*Fit a*	Common trend line (3+)	31.9 ± 0.1	0.72	
(Na^+)	*Fit c*	4+	44.6 ± 0.2	0.78	
	Fit e	5+	56.8 ± 0.2	0.92	
	Fit f	6+	62.0 ± 0.0	0.95	
	Fit g	7+	65.1[5] ± 0.4	0.98	
	Fit h	8+	66.5[5] ± 0.6	0.99	
	Fit i	9+	67.4[5] ± 0.6		
Linear PCL[3]	*Fit a*	Common trend line (2+ to 4+)	62.8 ± 0.5	0.90	0.77
(K^+)	*Fit b*	2+	70.0 ± 9.6	0.86	
	Fit c	3+ and 4+ trend	81.6 ± 0.9	0.90	
	Fit d	4+	90.7 ± 1.4		
4-Arm star PCL[2]	*Fit a*	Common trend line (2+ to 4+)	63.3 ± 0.5		0.78
(K^+)	*Fit c*	3+ and 4+ trend	81.4 ± 0.6	0.92	
	Fit d	4+	88.0 ± 1.6		
6-Arm star PCL[2]	*Fit a*	Common trend line (2+ to 4+)	64.5 ± 0.4	0.88	0.88
(K^+)	*Fit b*	3+ and 4+ trend	73.5 ± 0.9	0.88	
	Fit c	4+	83.7 ± 1.5		

[1] The values of the *A* fitting parameters are given with their 95% confidence interval.

[2] For plots with the constrained power fit functions (*pow = 0.66*) see **Figs. SI4** and **SI6–SI8**.

[3] See **Fig. 3**.

[4] Fit begins to poorly follow the data points (ratios tend to increase towards 1, *cf.* text for details).

[5] Fit only poorly follows the data points (parameter *A* ratios ~1, *cf.* text for details).

[6] The reported values are related to plots with the constrained power fit functions (*pow = 0.66*) of calcium-cationized complexes see **Fig. SI5**.

3.6. INTERPRETATION OF PARAMETER A RATIOS DIFFERING FROM 0.9

Extracting experimental CCS values from IM-MS measurements can lead to missing data points for any reason (e.g., small mass dispersity of a polymer yielding an insufficient *m/z* range coverage, suppression of ionization, lacking IM and/or MS resolving power). Fitting the CCS evolutions and calculating the ratios of successive parameters *A* allows detecting these missed or skipped CCS trends.

PEtP with 1–8 sodium cations has been analyzed ranging from oligomers (DP 1) to polymers containing up to 59 monomer units (BzO- and –H chain ends). The starting hypothesis is that no structural rearrangement or CCS trend has been missed within the investigated DP range. If the hypothetical next CCS trend (next power fit) was skipped during a structural rearrangement, the parameter A ratio should be significantly different from 0.9. The calculation of the $A_{Trend\ n}/A_{Trend\ (n+1)}$ ratios thus indicates how the CCS trend before or after a structural rearrangement from one trend with constant apparent density to another one should evolve.

Fig. 1 (and **Fig. SI4**) exemplifies the ratio $A_{Trend\ n}/A_{Trend\ (n+1)}$ interpretation on the structural evolutions of $[PEtP+3Na^+]^{3+}$ and $[PEtP+4Na^+]^{4+}$ complexes. For polymers smaller than DP 17, $[PEtP+3Na^+]^{3+}$ is following the CCS trend named '*fit b*' on **Fig. 1**, and after the structural rearrangement (DP > 21), the

Published in : Methods (2018), vol. 144, pp. 125–133
DOI: 10.1016/j.ymeth.2018.03.010
Status : Postprint (Author's version)

CCSs of the $[PEtP+3Na^+]^{3+}$ complexes follow the common trend line named '*fit a*'. The calculation of the parameter A ratio $A_{Trend\ n}/A_{Trend\ (n+1)}$ as $A_{fit\ a}/A_{fit\ b}$ yields the expected value of around 0.9 (*cf.* **Table 2**). On the contrary, calculating the ratio $A_{fit\ a}/A_{fit\ c}$ provides a value around 0.8 (ratio of the common trend line '*fit a*' of $[PEtP+4Na^+]^{4+}$ for DP > 44 equivalent to $A_{Common\ Trend\ line}$ and of the CCS trend of $[PEtP+4Na^+]^{4+}$ at DP < 36 ('*fit c*'; $A_{fit\ c}$)). This value suggests that a hypothetical CCS trend with an intermediate apparent density was skipped by $[PEtP+4Na^+]^{4+}$ during its structural rearrangement. This skipped CCS trend of the $[PEtP+4Na^+]^{4+}$ ions could be associated to the $[PEtP+3Na^+]^{3+}$ trend '*fit b*'. The skipping of a CCS trend is in agreement with the product of the two ratios of these consecutive CCS trends, e.g., $A_{fit\ a}/A_{fit\ b}$ (~0.9) multiplied by $A_{fit\ b}/A_{fit\ c}$ (~0.9), yielding 0.8 for $A_{fit\ a}/A_{fit\ c}$.

Additionally, it can be noted that the parameter *A* ratio values hold up when changing from alkali metal ions to alkaline earth metal ions, such as calcium cations. The parameter *A* ratio of the common trend line, i.e., the CCS trend of $[PEtP+1Ca^{2+}]^{2+}$, and of the 4+ ion CCS trend, as yielded by $[PEtP+2Ca^{2+}]^{4+}$ complexes, yields ~0.8 (see **Table 2** and **Fig. SI5**). This value is identical to the ratio calculated for $[PEtP+2Na^+]^{2+}$ and $[PEtP+4Na^+]^{4+}$ apparent density trends. A calcium adduct provides the same behavior in terms of CCS trends as the adduct of 2 sodium cations on the same polymer chain.

3.7. PREDICTING THE CCS TRENDS USING THE PARAMETER *A* RATIOS AND THE COMMON TREND LINE: APPLICATION TO PEO AND PCL TOPOLOGIES AND OUTLOOK FOR DATA TREATMENT AUTOMATION

Fig. 2 (and **Fig. SI6**) represents the CCS trends and their fits of poly(ethylene oxide) complexes carrying sodium cations. Once the CCS trend of the common trend line is established ('*fit a*'; the most compact trend), all other CCS trends with constant apparent density can be predicted by using the identified value from the parameter *A* ratio, i.e., 0.9. Decreasing the apparent density i.e., the parameter *A* by 10% from fit to fit predicts the trends of '*fit b*' to '*fit i*'. Aside from the structural rearrangements and assuming that e.g., no multimer formation took place during the experiments, all predicted trends with constant apparent density should be covered by experimental data points of polymer-cation complexes at different charge states.

The ratio calculation $A_{fit\ a}/A_{fit\ c}$ and $A_{fit\ c}/A_{fit\ e}$ of PEO being ~0.8 instead of the expected 0.9, we can strongly suspect that the two CCS trends '*fit b*' and '*fit d*' have been missed (see **Table 2**). This is due to the PEO sample's mass dispersity not covering a large enough DP range. The end and the beginning of these two missed trends are observed from DP 90 to 100 for $[PEO+3Na^+]^{3+}$ or around DP 135 for $[PEO+4Na^+]^{4+}$ ('*fit b*') and at DPs >130 for $[PEO+5Na^+]^{5+}$ ('*fit d*'), respectively. These two missing but predicted CCS trends were experimentally detected by Larriba and coworkers using a larger DP coverage of PEO [9], standing in good agreement with our data.

The CCS trend predictions hold as well on different topologies of poly(caprolactone) PCL (see linear PCL in **Fig. 3**, 4-arm star PCL in **Fig. SI7** and 6-arm star in **Fig. SI8**). For this purpose, the different topologies should cover a DP range large enough, notably including the common trend line, in order to establish appropriate trend predictions for the different charge states. Here, an additional difference between the polymers is that different topologies can cover different trends with constant apparent density with identical charge states (**Table 2**).

Published in : Methods (2018), vol. 144, pp. 125–133
DOI: 10.1016/j.ymeth.2018.03.010
Status : Postprint (Author's version)

For illustration purposes, the predicted trends '*fit b*' are covered by the 2+ complexes for the linear and the 4-arm star PCL complexes $[PCL_{Linear\ or\ 4\text{-}arm\ star}+2K^+]^{2+}$ (**Figs. 3** and **SI7**). The '*fit c*' trends are represented by their 3+ complexes $[PCL_{Linear\ or\ 4\text{-}arm\ star}+3K^+]^{3+}$. These interpretations can be retraced through the parameter *A* ratio calculations as $A_{fit\ a}/A_{fit\ b}$ ($A_{Common\ Trend\ line}/A_{Trend\ 2+}$) which yield ratio values around 0.9. Similarly, the ratios $A_{fit\ a}/A_{fit\ c}$ ($A_{Common\ Trend\ line}/A_{Trend\ 3+}$) provide values around 0.8. However for the 6-arm star PCL, no CCS trend specific to only the $[PCL_{6\text{-}arm\ star}+2K^+]^{2+}$ complexes could be found (see **Fig. SI8**). Instead, the $[PCL_{6\text{-}arm\ star}+2K^+]^{2+}$ complexes share the same CCS trend as the [PCL6-arm star+1K+]1+complexes. [PCL6-arm star+3K+]3+ complexes cover the predicted CCS trend '*fit b*', which was previously covered by the 2+ complexes for the linear and 4-arm star PCL topology counterparts. The ratio $A_{fit\ a}/A_{fit\ b}$ ($A_{Common\ Trend\ line}/A_{Trend\ 3+}$) of the [PCL6-arm star+3K+]3+ complexes again yields ~0.9.

It is interesting to note that in a recently published study from our group on multiple co-existing conformations of poly(acrylamide) in vacuo, the co-existing conformations (for an identical charge state) yielded as well CCS trends with 10% apparent density differences [17].

The fit parameter *A* ratio calculation is thus a powerful tool in the data processing which allows the prediction of missed CCS trends with constant apparent density or of inexistent CCS trends for given charge states (e.g., $[PCL_{6\text{-}arm\ star}+2K^+]^{2+}$ complexes at very low DP; not having a physical meaning). Differences in behaviors of polymer systems when changing either the monomer units or the polymer branching are easily and rapidly identifiable. The trend predictions could also be used as verification step when automating data processing for polymer mixture analyses. Indeed, once the parameter *A* of the common trend line is known, the trend predictions can be established and automated data treatment could verify its results. Multimer formation [18,19] or the presence of multiple polymer topologies could thus be detected through deviations from the trend predictions. IM-MS topology standards should nevertheless also be separately acquired in order to further verify any potentially identified deviation from the trend predictions, especially in the case of monodisperse biopolymer foldings studied by IM-MS. Moreover, deviations from the predicted trends due to structural rearrangements (tipping points) or due to acute three-dimensional structure differences could be confirmed through the here-developed method. With this method, only the parameter *A* of the common trend line has to be known to perform trend predictions. Data processing software could rely on such predictions, coupled to e.g., an RMSD approach, in order to automatically assist data extraction and to verify the consistency of the results.

3.8. NOTE CONCERNING THE UNCONSTRAINED POW PARAMETERS AND PARAMETER *A* RATIOS

CCS trends can also be performed successfully outside the postulate of the constrained *pow = 0.66* fit parameter (**Eq. (2)**). This was done for linear and 6-arm star PCL polymers with potassium adducts (**Figs. SI9** and **SI10**). It is still possible to perform the strategy of calculating parameter *A* ratios from one charge state to the next as long as the condition of comparing polymers with similar shapes is respected (close/similar pow parameter values).

Published in : Methods (2018), vol. 144, pp. 125–133
DOI: 10.1016/j.ymeth.2018.03.010
Status : Postprint (Author's version)

3.9. *POW = 0.66* AT HIGHER CHARGE STATES

At higher charge states, the constrained *pow = 0.66* trends begin to deviate from the experimental CCS evolutions. For example, the CCS evolutions of the 7+, 8+ and 9+ charge states of PEO do not correlate well with the constrained *pow = 0.66* fit function (see **Table SI2** and **Fig. SI6**). When nevertheless applying the constrained *pow = 0.66* fits to these CCS evolutions, the here-developed prediction and interpretation method still holds up.

The *pow = 0.66* parameter being to-date exclusively associated with near-spherical shapes [28], together with more detailed interpretations and explanations of the higher charge states where the fits begin to poorly fit with *pow = 2/3* will be the subject of a future paper.

3.10. FROM FITTING CCS TRENDS TO FITTING DRIFT TIME OR MOBILITY DATA

The CCS fit methodology can be extended from CCS evolutions to drift time and mobility (K_0) evolutions.

The power law fits of CCS evolutions plotted as a function of the DP (or mass) become linear fit functions when working with drift time evolutions [38] (**Fig. SI11**).

Given the Mason-Schamp equation (**Eq. (1)**), the graphs of the charge *z* divided by the mobility K_0 (z/K_0) plotted as a function of the DP (or mass) will yield the same power law (*pow* ~*2/3*) trends as for CCS evolutions. In this case, the parameter *A* will not directly reflect an apparent density but an apparent mobility contribution of the monomers to the complexes in the gas phase.

Lastly, when working with CCS evolutions, linear fits can as well be used instead of the power law fits if fulfilling specific conditions. Linear fits could be used for CCS evolutions if the data set does not cover a large mass range and if the masses are not too close to the (0,0) coordinate intercept because of the convergence of both the linear and the power law functions within a limited mass range (see **Fig. 1**). In this case, the approximation of using linear fits without (0,0) interception in CCS vs. mass plots could be valid [41]. Nevertheless, larger data sets, and especially if extrapolating data interpretation, require power law fits in order to understand the CCS evolutions as a function of the mass.

4. Conclusions

Five different synthetic homopolymers were used to develop an Ion Mobility data fitting method. Each CCS trend of each charge state of the polymer-cation complexes can be fitted using a power law fit function ($CCS = A.DP^{pow}$). Structural information yielded by Ion Mobility can thus be extracted as its two fitting parameters *A* and *pow*. This work deals with the parameter *A* while the pow parameter will be the subject of a specifically dedicated work. The data fitting and prediction method relies on experimental data only, without any computational chemistry *a prioris*. We showed that the CCS trends follow *apparent spherical tendencies* (apparent isotropic growth), exhibiting a *pow* fitting parameter of around *0.66* (*2/3*). Then, constraining the power fits to *pow = 0.66* allowed merging all IM information into one single parameter: the fit parameter *A*. This parameter reflects the average volume occupied by the monomers when the mass of the polymer increases for each charge state. The

Published in : Methods (2018), vol. 144, pp. 125–133
DOI: 10.1016/j.ymeth.2018.03.010
Status : Postprint (Author's version)

parameter *A* of each trend can hence be interpreted as an apparent density, resulting in the interpretation of IM-MS results, i.e. the CCS evolutions, as trends with constant apparent density (see **Eq. (8)**). The lowest charge state (singly charged ions) presented the most compact structure. It reflects the trend with the highest apparent density defined in this work as the common trend line. Higher charge states yielded different trends with constant apparent density. These CCS evolutions merged with higher density trends for growing polymer chains (DP) until they eventually merged with the common trend line. All these evolutions fit with different, trend-specific, parameter *A* values.

The methodology of using power law fits with constrained *pow* parameters, reducing the fit equation to one single fitting parameter, allowed the calculation of parameter *A* ratios of successive CCS trends of the different charge states. These ratios were found to be constant (~0.9 for alkali metal cations – 10% in density difference) between successive CCS trends unless the CCS trends were experimentally skipped. It could as well be noted that doubly charged alkaline earth cations (e.g., Ca^{2+}) provided identical results to the alkali cations when equivalent charge states were considered.

Given the constancy of the parameter *A* ratios, predictions of (missed or inexistent for given charge states) CCS trends with constant apparent density could easily be performed. Deviations from the constancy of these ratios or deviations from these predicted CCS trends could be used as analytical quantifiers to detect and verify anomalies in unknown polymer samples. Such anomalies could include differences in behaviors of polymer systems due to differing polymer topologies, folding or differing monomer units. The occurrence of structural rearrangements, of acute three-dimensional structure differences of the polymer-cation complexes, or the presence of multimer complexes could be verified and confirmed using the predicted trends with constant apparent density.

Identically, biomolecules also exhibit IM-MS results dependent on their apparent densities [41–43]. The apparent densities allow the interpretation without any *a priori* on the three-dimensional shape of the biomolecule ions. Deviations from the constancy of the parameter *A* ratios when increasing the charge state of given biomolecules could also indicate changes in their folding pattern.

The prediction method could also be used in data processing software to automatically assist data extraction or verification.

The power law fit methodology could be extended from the CCS evolutions to drift time (linear fits) and ion mobility (K_0) evolutions (z/K_0 with power fits).

The parameter *A* from **Eqs. (2)** or **(8)** is strongly related to the physicochemical properties (e.g., charge solvation capacity) of the monomer units constituting the polymers. Further investigating the parameter *A* should provide deeper physicochemical information and should in turn assist the choice of an appropriate initial guess for computational chemistry (such as calculation methods, interaction potential choices, charge placements). A future paper will identify the shape information contained in the *pow* parameter. Finally, the next step in the data prediction strategy will be to expand the predictions from synthetic polymer systems to more complex biomolecular systems.

Published in : Methods (2018), vol. 144, pp. 125–133
DOI: 10.1016/j.ymeth.2018.03.010
Status : Postprint (Author's version)

Declaration of interest

None.

Acknowledgments

The authors acknowledge the financial support of the F.R.S.-FNRS (Jean R. N. Haler is a FRIA Doctorate Fellow). Philippe Massonnet (Mass Spectrometry Laboratory, ULiège) and Prof. Bernard Leyh (Molecular Dynamics Laboratory, ULiège) are acknowledged for their valuable discussions on this paper. The authors thank the Center for Education and Research on Macromolecules (CERM Laboratory, ULiège) for providing the polymers, especially Thomas Defize and Stéphan Carion. Dr. Benoît Clément and Dr. Stéphanie Vanslambrouck are thanked for their technical assistance and the discussions.

Appendix A. Supplementary data

MATERIALS & METHODS

CHEMICALS.

The solvents toluene, tetrahydrofuran (THF) and dichloromethane (CH_2Cl_2), used for the synthesis of (poly(2-ethoxy-1,3,2-dioxaphospholane 2-oxide); poly(ethoxyphosphate)[1], PEtP), were dried under vacuum before use. 2-Chloro-1,3,2-dioxaphospholane 2-oxide (COP) was purchased from Acros, diethyl ether, methanol (analytical grade) and calcium hydride (CaH_2) (Aldrich) were used as received. Ethanol (Aldrich), benzyl alcohol (Aldrich), N,N-diethylethanamine (or triethylamine, TEA) (Aldrich), and 1,8-diazobicyclo[5.4.0]undec-7-ene (DBU) (Aldrich) were dried over calcium hydride at room temperature, followed by distillation under vacuum before use. 1-1-[3,5-Bis(trifluoromethyl)phenyl]-3-cyclohexyl-2-thiourea (TU) was synthesized as described elsewhere[2].

SYNTHESIS OF THE MONOMER (EP).

The monomer (2-ethoxy-1,3,2-dioxaphospholan 2-oxide, EP) for the PEtP synthesis was synthesized as described by Clément *et al.*[1]. The reaction is based on an esterification reaction of the chlorinated cyclic precursor 2-chloro-2-1,3,2-dioxaphospholan 2-oxide (COP).

The solvent and reagents used were dried either by a drying apparatus or by fresh distillations. COP (0.7 mol) in 200 mL of dry tetrahydrofurane (THF) was added dropwise (during 1-2 h) under N_2 atmosphere to a mixture of ethanol (EtOH 0.7 mol), triethylamine (TEA) (0.7 mol) in 200 mL of dry THF. The final conditions were COP/EtOH/TEA 1/1/1. The reaction flask was kept at 0 °C under constant stirring during the reaction time of 4 to 5 hours. After the reaction was completed, the reaction medium was filtered under ambient atmosphere in order to remove the precipitated salt. The product was dried under vacuum and kept under N_2 atmosphere at 20 °C for one night. Afterwards, a fractional

Published in : Methods (2018), vol. 144, pp. 125–133
DOI: 10.1016/j.ymeth.2018.03.010
Status : Postprint (Author's version)

distillation was performed under vacuum (~3 h, oil bath at 130 °C - 140 °C). The observed boiling point of the monomer was around 74 °C.

SYNTHESIS OF THE POLY(PHOSPHOESTER) (POLY(2-ETHOXY-1,3,2-DIOXAPHOSPHOLANE 2-OXIDE; PETP).

The polymer synthesis was inspired by Clément and coworkers[1]. The polymers were synthesized by Ring-Opening Polymerization (ROP) with a dual organo-catalysis system (1,8-diazobicyclo[5.4.0]undec-7-ene DBU and 1-1-[3,5-bis(trifluoromethyl)phenyl]-3-cyclohexyl-2thiourea TU) as initially described by Hedrick and coworkers[3,4]. Several linear poly(2-ethoxy-1,3,2-dioxaphospholane 2-oxide) (poly(ethoxyphosphate); PEtP) (PEtP 1200 g/mol, 3000 g/mol, 4500 g/mol, 5500 g/mol; **Figure SI1**) were produced.

For the 1200 g/mol and 3000 g/mol polymers, 2-ethoxy-1,3,2-dioxaphospholan 2-oxide (EP) (39.4 mmol) was mixed with TU (5% of EP, 1.97 mmol) in dry CH_2Cl_2 (40 mL) in order to obtain a 1 M solution. Before adding the solvent (CH_2Cl_2), three azeotropic distillations with anhydrous toluene were performed to eliminate residual traces of water. The freshly distilled initiator was then added (benzyl alcohol, BzOH, 1.97 mmol). The ratio EP/BzOH was fixed according to the intended Degree of Polymerization (DP). The polymerization-initiating catalyst, DBU, was then added (2.7 mmol) to the reaction medium at 0 °C under constant stirring. The quantity of DBU was chosen according to the molar ratio DBU/BzOH to lie within 1.2 and 1.5. After 15 minutes for PEtP 1200 g/mol or after 40 minutes for PEtP 3000 g/mol, the polymerizations were stopped by precipitating the reaction medium in cold diethyl ether under heavy stirring. The polymers were then recuperated while being solid. They were dried under vacuum and put under N_2 atmosphere.

The longer polymers (4500 g/mol and 5500 g/mol) were obtained using a slightly different procedure. Toluene was used as solvent and the monomer concentration was raised to 4 M. The ratio DBU/TU was set to 1/1. The ratio DBU/BzOH was kept at 1.5 equivalents of DBU towards 1 equivalent of the initiator. Instead of the azeotropic distillations, TU was dried overnight under vacuum. After the polymerization, the polymer was precipitated in cold diethyl ether and was dried under vacuum in order to be stored under N_2 atmosphere.

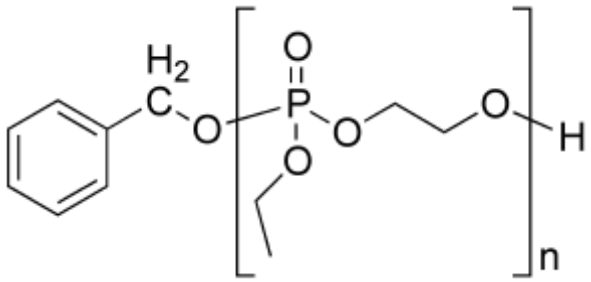

Figure SI1: Poly(ethoxyphosphate) (poly(2-ethoxy-1,3,2-dioxaphospholane 2-oxide), PEtP).

Published in : Methods (2018), vol. 144, pp. 125–133
DOI: 10.1016/j.ymeth.2018.03.010
Status : Postprint (Author's version)

ION MOBILITY-MASS SPECTROMETRY.

The PEtP and PEO samples were infused at a flow rate of 4 µL/min, using a syringe pump and a 250 µL Thermo Scientific syringe, into a SYNAPT G2 HDMS Ion Mobility-Mass Spectrometer (Waters, Manchester, UK) which was used to determine the Arrival Time Distributions. This IM-MS is fitted with an Electrospray Ionization (ESI) source and a stacked ring Traveling Wave (T-Wave) Ion Mobility cell. The capillary voltage was set to 3 kV, the sampling cone voltage was 40 V and the extraction cone was set to 4 V. The source and desolvation temperatures were 100 °C and 200 °C respectively. No cone gas flow was used and the desolvation gas flow was set to 500 L/h. The voltages for the trap and the transfer Collision Energies (CE) were set to 4 V and 2 V, respectively and the trap bias was set to 45 V. The IM wave height was 40 V and the wave speed was set to 1200 m/s. The trap Ar gas flow was set to 2 mL/min, the He gas flow was 180 mL/min and the N_2 pressure in the IM cell was set to 2.6 mbar.

COLLISION CROSS-SECTION (CSS)/ION MOBILITY CALIBRATION.

As Traveling Wave Ion Mobility cells need to be calibrated in order to convert drift time measurements into CCS values, the calibration methodology described by Ruotolo and coworkers was followed[5] using proteins and peptides as calibrants (bradykinin[6], tryptic digest of Bovine Serum Albumin (BSA)[7], ubiquitin[8], myoglobin[9], cytochrome C[10] and lysozyme[11]; see **Figure SI2**, **Figure SI3** and **Table SI1**).

PCL calibration curves are to be found in the paper of Morsa *et al.*[12].

Even if the T-Wave (Traveling Wave Ion Mobility) conditions were identical for PEtP and PEO, two different calibration sets were used.

The blue lines in **Figure SI2** and **Figure SI3** correspond to the 95% confidence bands; the red lines correspond to the 95% prediction bands. Not all the molecules described in **Table SI1** were used for both calibrations.

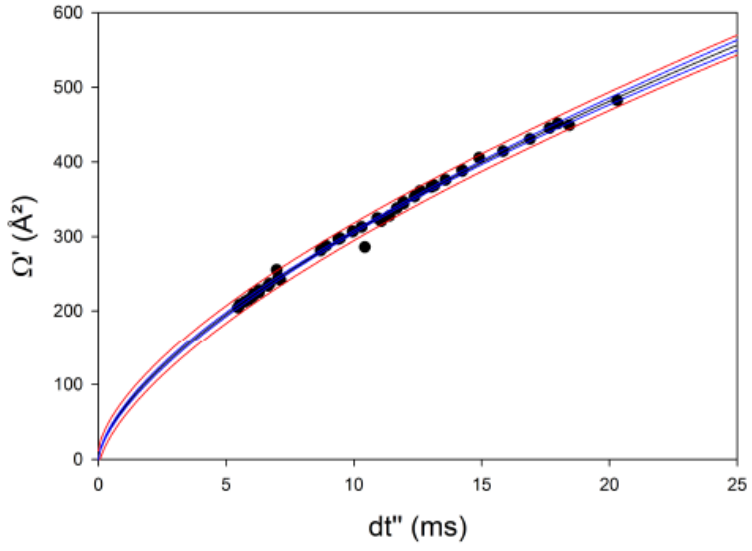

Figure SI2: Calibration curve to convert drift times into CCS values (as T-Wave derived CCS) for PEtP polymer complexes. The power fit function is used to establish the calibration curve ($\Omega' = a.dt''^{b}$). The fit parameters of the calibration curve are $a=68.3367$ and $b=0.6516$; the fit parameters of the 95% prediction band are $a=61.6784$ and $b=0.6773$.

Published in : Methods (2018), vol. 144, pp. 125–133
DOI: 10.1016/j.ymeth.2018.03.010
Status : Postprint (Author's version)

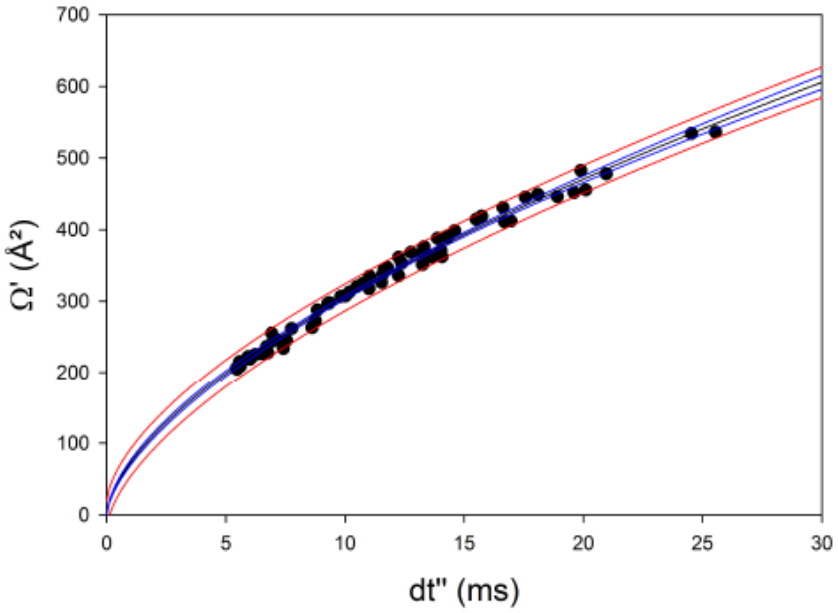

Figure SI3: Calibration curve to convert drift times into CCS values (as T-Wave derived CCS) for PEO polymer complexes. The power fit function is used to establish the calibration curve ($\Omega' = a.dt''^{b}$). The fit parameters of the calibration curve are $a=72.6837$ and $b=0.6234$; the fit parameters of the 95% prediction band are $a=62.1956$ and $b=0.6606$.

Table SI1: Table of proteins and peptides used to calibrate the Traveling Wave Ion Mobility.

Molecule	Mass (Da)	z	m/z	Ω (Å², CCS) in He
Bradykinin	1059.62	2	530.81	246
FPK	390.23	1	391.23	123.14
YTK	438.23	1	439.23	131.96
VGTR	431.26	1	432.26	136.71
ADLAK	516.29	1	517.29	159.31
AFDEK	608.29	1	609.29	168.36
IETMR	648.33	1	649.33	181.29
KFWGK	664.37	1	665.37	185.85
VASLR	544.34	1	545.34	163.7
SEIAHR	711.37	1	712.37	181.53
TPVSEK	659.35	1	660.35	175.98
ATEEQLK	817.42	1	818.42	206.4
LVTDLTK	788.46	1	789.46	205.76
AEFVEVTK	921.49	1	922.49	223.42
YLYEIAR	927.00	1	927.99	228.03
LVVSTQTALA	1001.58	1	1002.58	239.27
LVTDTDLTK	788.5	2	395.25	205
GACLLPK + CAM	757.48	2	379.74	207

Published in : Methods (2018), vol. 144, pp. 125–133
DOI: 10.1016/j.ymeth.2018.03.010
Status : Postprint (Author's version)

ATEEQLK	817.46	2	409.73	209
LCVLHEK+CAM	897.52	2	449.76	228
AEFVEVTK	921.52	2	461.76	219
YLYEIAR	926.52	2	464.26	237
LVVSTQTALA	1001.62	2	501.81	234
QTALVELLK	1013.66	2	507.83	245
LVNELTEFAK	1162.68	2	582.34	262
HLVDEPQNLIK	1304.78	2	653.39	288
TVMENFVAFVDK	1398.72	2	700.36	297
SLHTLFGDELCK + CAM	1418.76	2	710.38	297
YICDNQDTISSK + CAM	1442.7	2	722.35	298
LGEYGFQNALIVR	1478.86	2	740.43	307
DDPHACYSTVFDK + CAM	1553.72	2	777.86	313
MPCTEDYLSLILNR + CAM	1723.88	2	862.94	338
YNGVFQECCQAEDK + CAM	1748.72	2	875.36	325
HLVDEPQNLIK	1304.76	3	435.92	319
SLHTLFGDELCK + CAM	1291.65	3	431.55	334
TCVADESHAGCEK+CAM	1461.75	3	488.25	340
DDPHACYSTVFDK+CAM	1248.63	3	417.21	323
KVPQVSTPTLVEVSR	1638.99	3	547.33	338
DAFLGSFLYEYSRR	1722.75	3	575.25	383
DAIPENLPPLTADFAEDKDVCK+CAM	2460.2	3	820.07	422
QNCDQFEKLGEYGFQNALIVR	2474.2	3	824.73	429
NECFLSHKDDSPDLPK	1900.96	4	476.24	442
Ubiquitin	8560.8	7	1223.82	1580
Ubiquitin	8560.8	8	1070.97	1622

Published in : Methods (2018), vol. 144, pp. 125–133
DOI: 10.1016/j.ymeth.2018.03.010
Status : Postprint (Author's version)

Ubiquitin	8560.8	9	952.2	1649
Ubiquitin	8560.9	10	857.09	1732
Ubiquitin	8561.08	11	779.28	1802
Myoglobin	16950.93	12	1413.58	3044
Myoglobin	16977.09	13	1304.93	3136
Myoglobin	16978.22	14	1211.73	3143
Myoglobin	16981.05	15	1131.07	3230
Myoglobin	16982.08	16	1060.38	3313
Myoglobin	16951.10	17	998.12	3384
Myoglobin	16950.6	18	942.7	3489
Myoglobin	16947.81	19	892.99	3570
Myoglobin	16948	20	848.4	3682
Myoglobin	16947	21	808	3792
Myoglobin	16940	22	771	3815
Cytochrome c	12230.07	5	2447.01	1340
Cytochrome c	12229.11	6	2039.18	1602
Cytochrome c	12371.9	10	1236.19	2226
Cytochrome c	12371.9	11	1123.9	2303
Cytochrome c	12375.96	12	1030.33	2335
Cytochrome c	12352.6	13	951.2	2391
Cytochrome c	12348.7	14	883.05	2473
Cytochrome c	12354.75	15	824.65	2579
Cytochrome c	12187.49	16	762.72	2679
Cytochrome c	12385.86	17	727.58	2723
Cytochrome c	12326.4	18	685.8	2766
Lysozyme	14303.73	6	2384.96	1355

Published in : Methods (2018), vol. 144, pp. 125–133
DOI: 10.1016/j.ymeth.2018.03.010
Status : Postprint (Author's version)

RESULTS & DISCUSSION

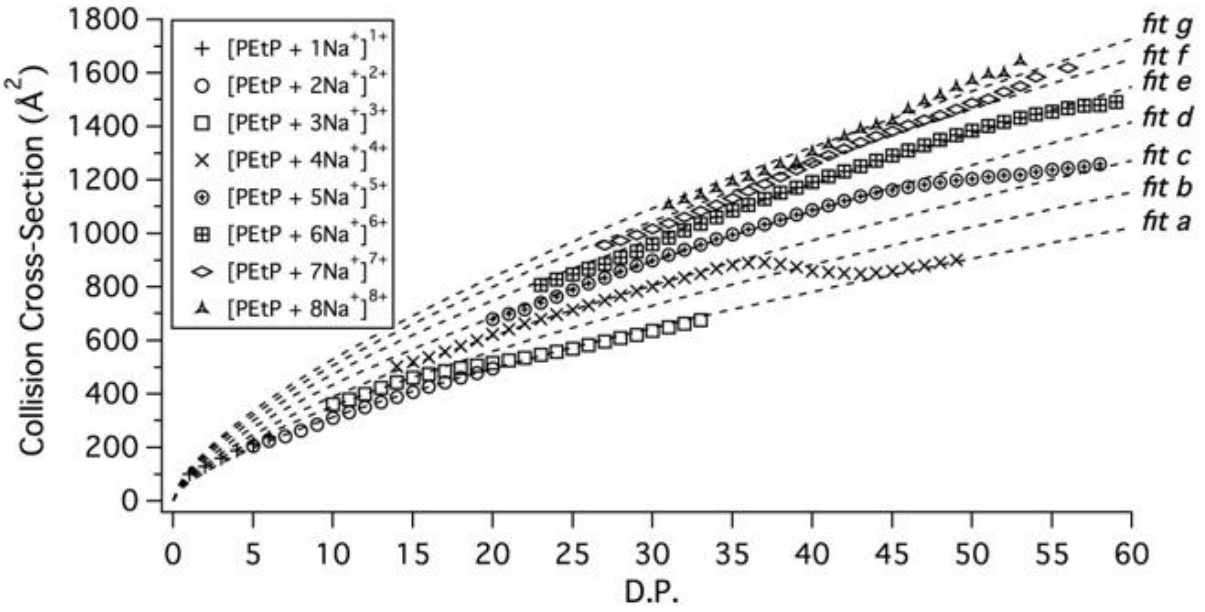

Figure SI4: Plot of the Collision Cross-Section (CCS, He-derived T-Wave$_{N2}$ CCS) versus the DP (Degree of Polymerization) of sodiated poly(ethoxyphosphate) (PEtP) polymer ions at different charge states (from 1+ to 8+). The constrained power fit functions ($CCS = A.DP^{pow}$, $pow=0.66$) for the different CCS trends before and after the tipping points are described as *fit a* to *fit g*.

Published in : Methods (2018), vol. 144, pp. 125–133
DOI: 10.1016/j.ymeth.2018.03.010
Status : Postprint (Author's version)

Table SI2: Fitting parameters of the trend lines for poly(ethoxyphosphate) PEtP, poly(ethylene oxide) PEO and different topologies of poly(caprolactone) PCL polymer-cation complexes. The unconstrained fits ($CCS = A.DP^{pow}$, **Equation 2**) are calculated with free *A* and *pow* parameters.

Polymer	Fitting Curve	Charge State Description	$pow^{(1)}$	$A^{(1)}$
PEtP[(2)]	*Fit a*	Common trend line (2+ to 4+)	0.67 ± 0.01	65.1 ± 2.1
	Fit b	3+	0.61 ± 0.04	88.4 ± 9.0
	Fit c	4+	0.63 ± 0.00	94.5 ± 1.4
	Fit d	5+	0.68 ± 0.01	88.9 ± 2.8
	Fit e	6+	0.71 ± 0.01	87.3 ± 3.2
	Fit f	7+	0.74 ± 0.01	80.5 ± 3.1
	Fit g	8+	0.76 ± 0.02	78.7 ± 7.4
PEO[(2)]	*Fit a*	Common trend line (3+)	0.64 ± 0.02	35.2 ± 4.1
	Fit c	4+	0.50 ± 0.03	93.6 ± 12.5
	Fit e	5+	0.58 ± 0.03	81.9 ± 13
	Fit f	6+	0.71 ± 0.01	49.6 ± 2.4
	Fit g	7+	0.83 ± 0.01	28.8 ± 1.8
	Fit h	8+	0.92 ± 0.01	18.8 ± 0.7
	Fit i	9+	0.93 ± 0.01	18.8 ± 0.7
Linear PCL[(3)]	*Fit a*	Common trend line (2+ to 4+)	0.75 ± 0.01	44.4 ± 1.1
	Fit b	2+	0.68[(4)]	67.9[(4)]
	Fit c	3+ and 4+ trend	0.64 ± 0.04	87.4 ± 12.4
	Fit d	4+	0.63[(4)]	101.8[(4)]
6-arm star PCL[(3)]	*Fit a*	Common trend line (2+ to 4+)	0.70 ± 0.01	53.6 ± 2.4
	Fit b	3+ and 4+ trend	0.63 ± 0.03	81.3 ± 10.6
	Fit c	4+	0.60[(4)]	103.6[(4)]

[(1)] The values of the pow and A fitting parameters are given with their 95% confidence interval.
[(2)] see **Figure 1** and **Figure 2**.
[(3)] see **Supplementary Information** (**Figure SI9** and **Figure SI10**).
[(4)] Fitted on small amount of data points; no 95% confidence interval calculation.

Published in : Methods (2018), vol. 144, pp. 125–133
DOI: 10.1016/j.ymeth.2018.03.010
Status : Postprint (Author's version)

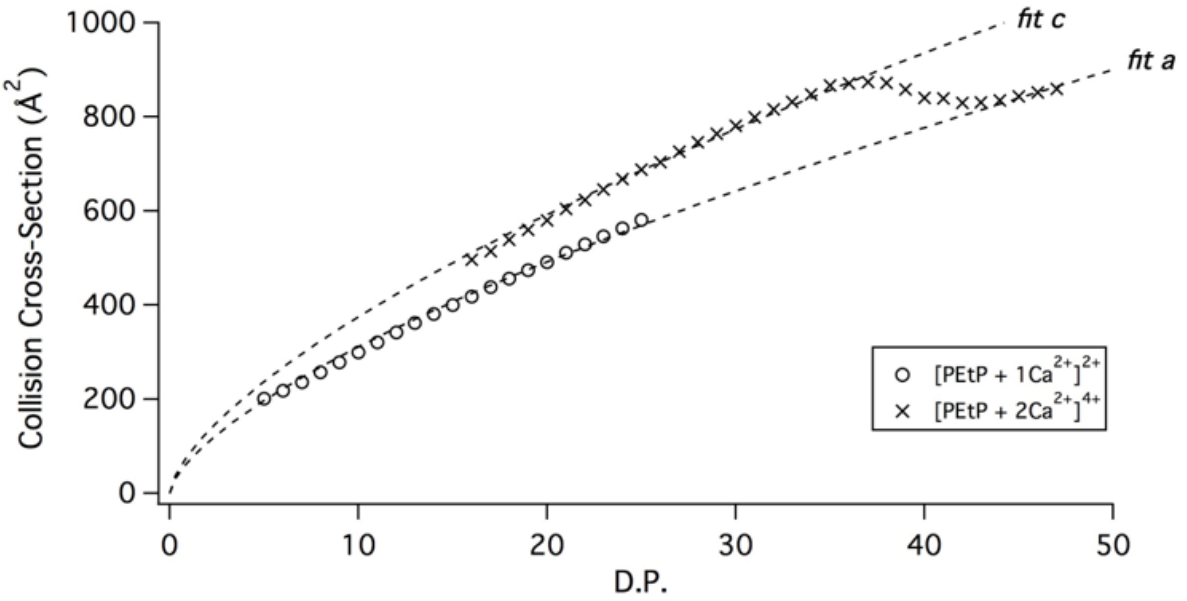

Figure SI5: Plot of the Collision Cross-Section (CCS, He-derived T-Wave$_{N2}$ CCS) versus the DP (Degree of Polymerization) of poly(ethoxyphosphate) (PEtP) polymers with one or two calcium cations. The constrained power fit functions (*CCS = A.DP^{pow}*, *pow=0.66*) for the two CCS trends are described as *fit a* (i.e. the common trend line) and *fit c*.

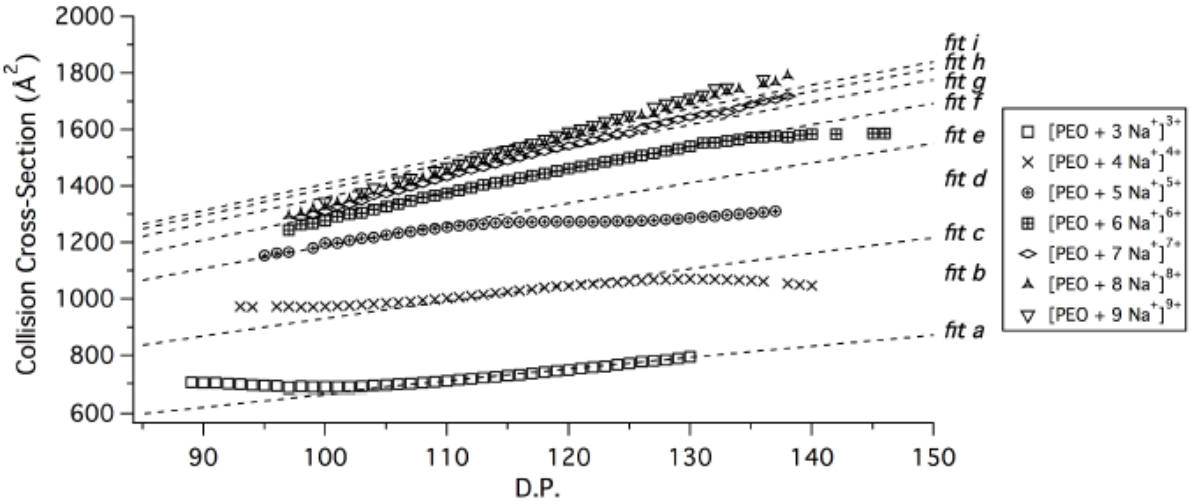

Figure SI6: Plot of the Collision Cross-Section (CCS, He-derived T-Wave$_{N2}$ CCS) as a function of the DP (Degree of Polymerization) of sodiated poly(ethylene oxide) (PEO) polymer ions (from 3+ to 9+). The constrained power fit functions (*CCS = A.DP^{pow}*, *pow=0.66*) for the different CCS trends before and after the tipping points are described as *fit a* to *fit i*. The fit functions *fit b* and *fit d* are not shown but are still accounted for in the plot as they denote the CCS trends missed in the analyzed DP range.

Published in : Methods (2018), vol. 144, pp. 125–133
DOI: 10.1016/j.ymeth.2018.03.010
Status : Postprint (Author's version)

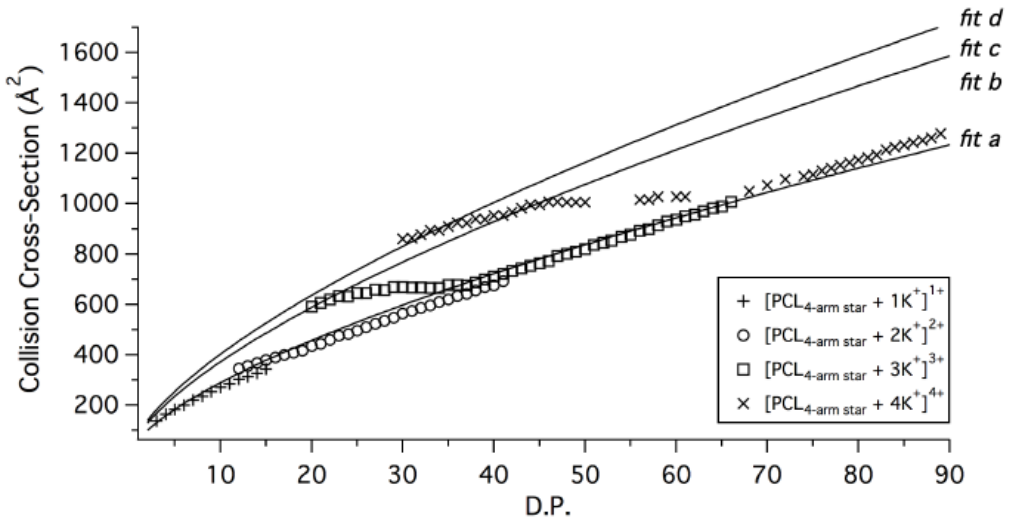

Figure SI7: Plot of the Collision Cross-Section (CCS, He-derived T-Wave$_{N2}$ CCS) as a function of the DP (Degree of Polymerization) of 4-arm star poly(caprolactone) (PCL) polymers with varying numbers of potassium cations used to reach different charge states (from 1+ to 4+). The constrained power fit functions (*CCS = A.DP^{pow}*, *pow=0.66*) for the different CCS trends before and after the tipping points are described as *fit a* to *fit d*. The fit function *fit b* is not shown but is still accounted for in the plot as it denotes the CCS trend of the 2+ complexes which did not yet reach the plateau (< DP 12). **Figure SI15** highlights the data points used for performing the data fits.

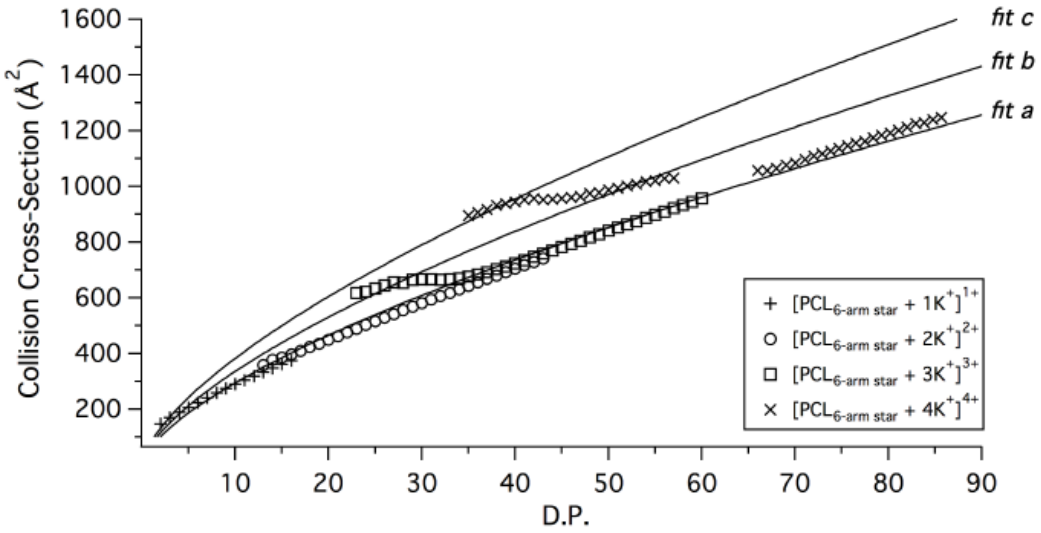

Figure SI8: Plot of the Collision Cross-Section (CCS, He-derived T-Wave$_{N2}$ CCS) as a function of the DP (Degree of Polymerization) of 6-arm star poly(caprolactone) (PCL) polymers with varying numbers of potassium cations used to reach different charge states (from 1+ to 4+). The constrained power fit functions (*CCS = A.DP^{pow}*, *pow=0.66*) for the different CCS trends are described as *fit a* to *fit c*. No new trend is yielded by the 2+ complexes which do not show a structural rearrangement. Figure SI16 highlights the data points used for performing the data fits.

Published in : Methods (2018), vol. 144, pp. 125–133
DOI: 10.1016/j.ymeth.2018.03.010
Status : Postprint (Author's version)

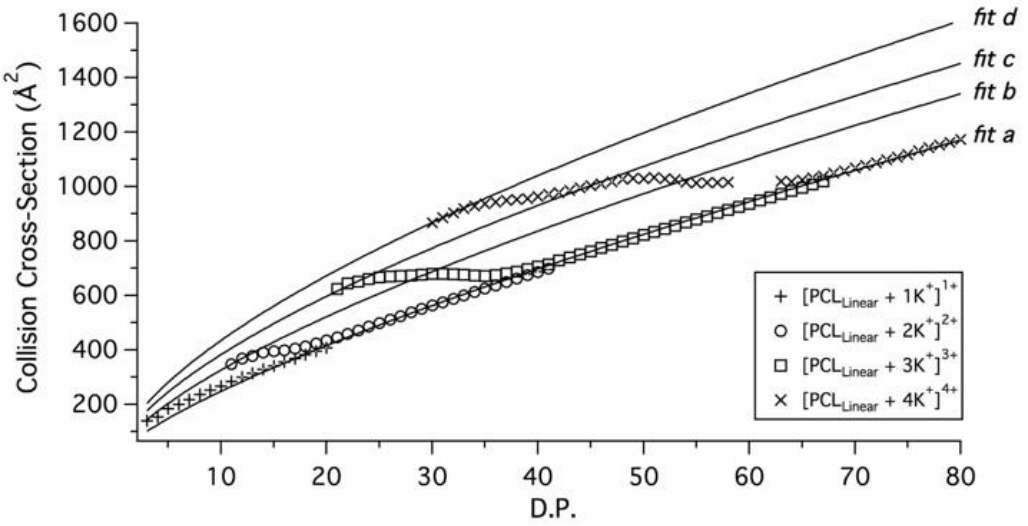

Figure SI9: Plot of the Collision Cross-Section (CCS, He-derived T-Wave$_{N2}$ CCS) versus the DP (Degree of Polymerization) of linear poly(caprolactone) (PCL) polymers with varying numbers of potassium cations used to reach different charge states (from 1+ to 4+). The unconstrained power fit functions (*CCS = A.DP^{pow}*, **Equation 2**) for the different CCS trends are described as *fit a* to *fit d*.

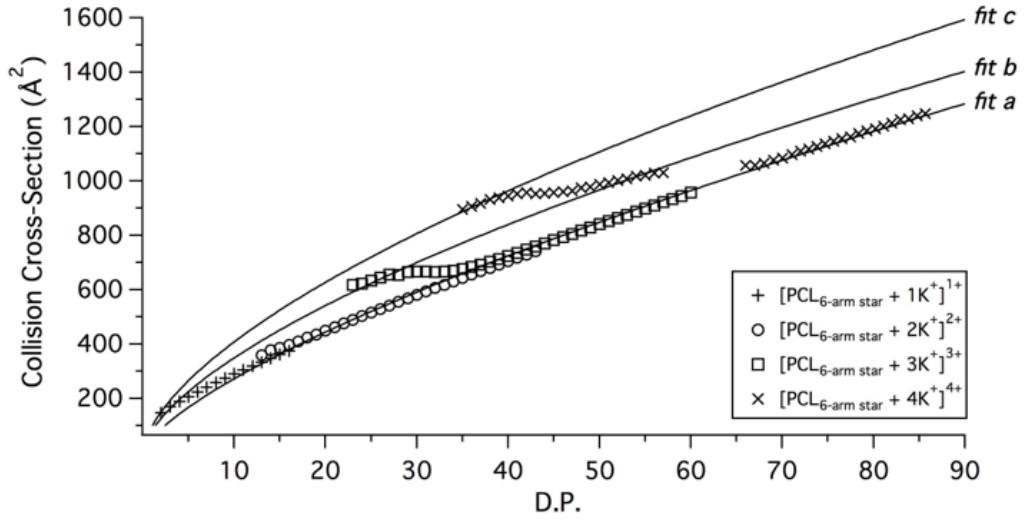

Figure SI10: Plot of the Collision Cross-Section (CCS, He-derived T-Wave$_{N2}$ CCS) as a function of the DP (Degree of Polymerization) of 6-arm star poly(caprolactone) (PCL) polymers with varying numbers of potassium cations used to reach different charge states (from 1+ to 4+). The unconstrained power fit functions (*CCS = A.DP^{pow}*, **Equation 2**) for the different CCS trends are described as *fit a* to *fit c*.

Published in : Methods (2018), vol. 144, pp. 125–133
DOI: 10.1016/j.ymeth.2018.03.010
Status : Postprint (Author's version)

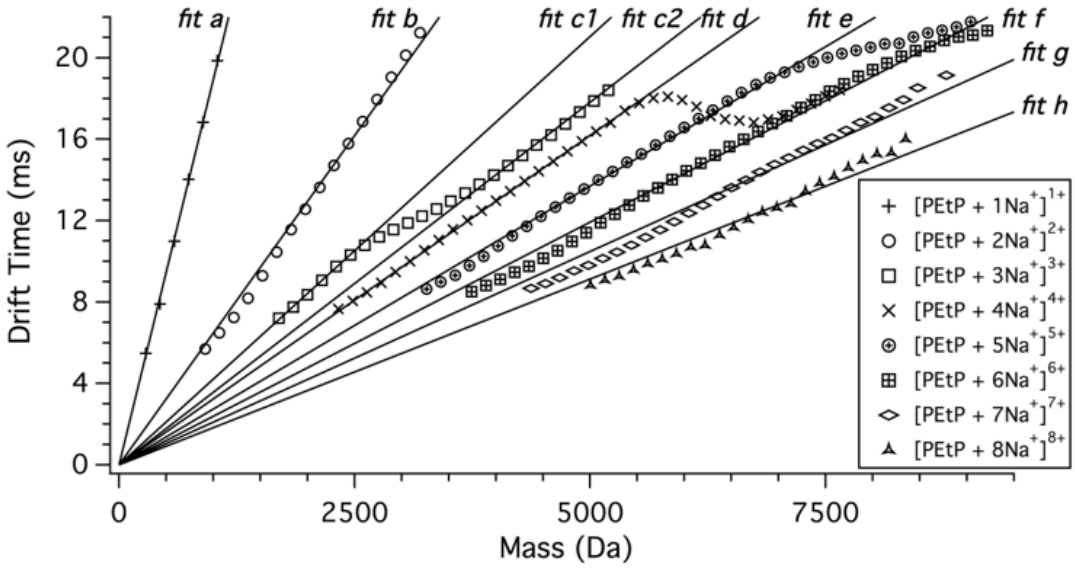

Figure SI11: Plot of the measured drift time as a function of the mass of poly(ethoxyphosphate) (PEtP) polymers with varying numbers of sodium cations used to reach different charge states (from 1+ to 8+). The constrained linear fit functions ($y = y_0+m.x$ and $y_0=0$) for the different CCS trends are described as *fit a* to *fit h*.

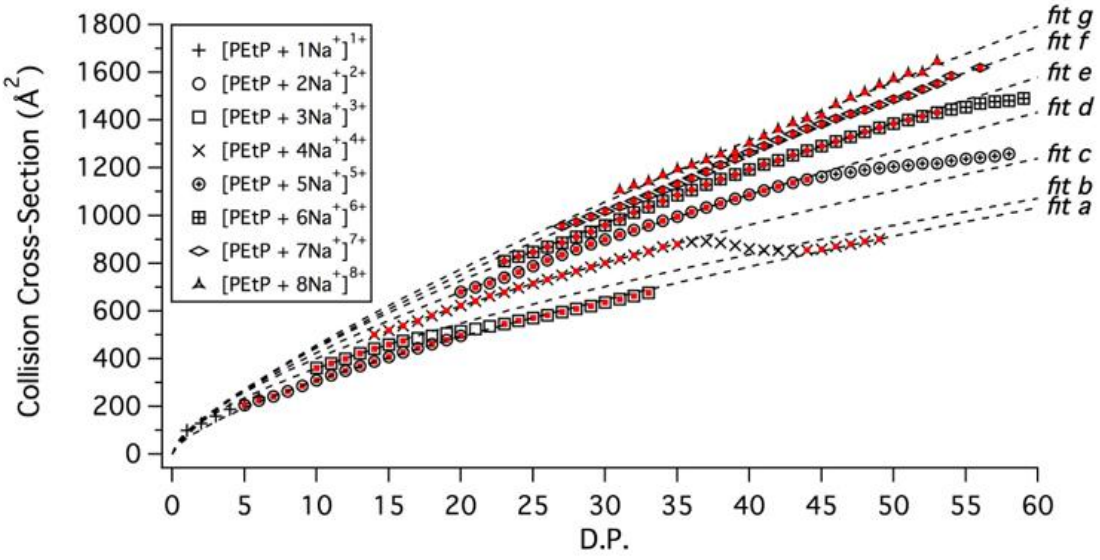

Figure SI12: Figure 1 (CCS vs. DP of PEtP) with highlighted data points (red dots) used for performing the data fits ($CCS = A.DP^{pow}$, *pow* unconstrained).

Published in : Methods (2018), vol. 144, pp. 125–133
DOI: 10.1016/j.ymeth.2018.03.010
Status : Postprint (Author's version)

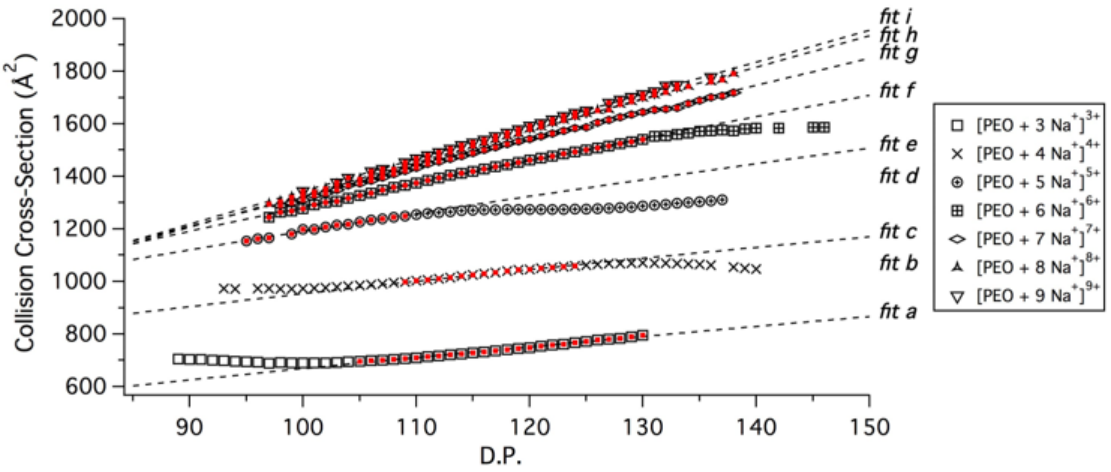

Figure SI13: Figure 2 (CCS vs. DP of PEO) with highlighted data points (red dots) used for performing the data fits (*CCS = A.DP^{pow}*, *pow* unconstrained).

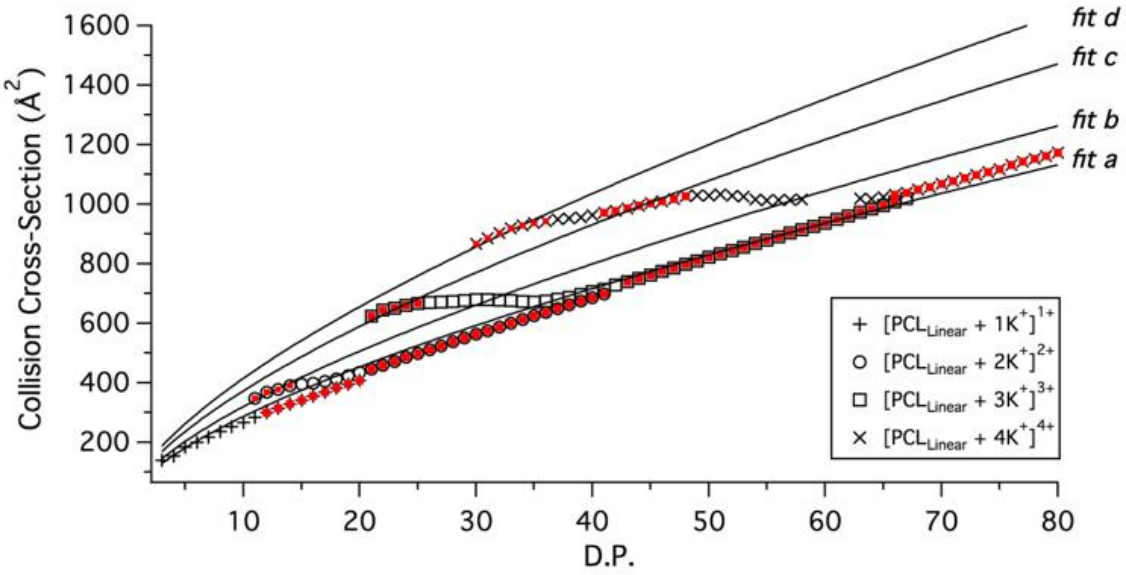

Figure SI14: Figure 3 (CCS vs. DP of linear PCL) with highlighted data points (red dots) used for performing the data fits (*CCS = A.DP^{pow}*, *pow=0.66*).

Published in : Methods (2018), vol. 144, pp. 125–133
DOI: 10.1016/j.ymeth.2018.03.010
Status : Postprint (Author's version)

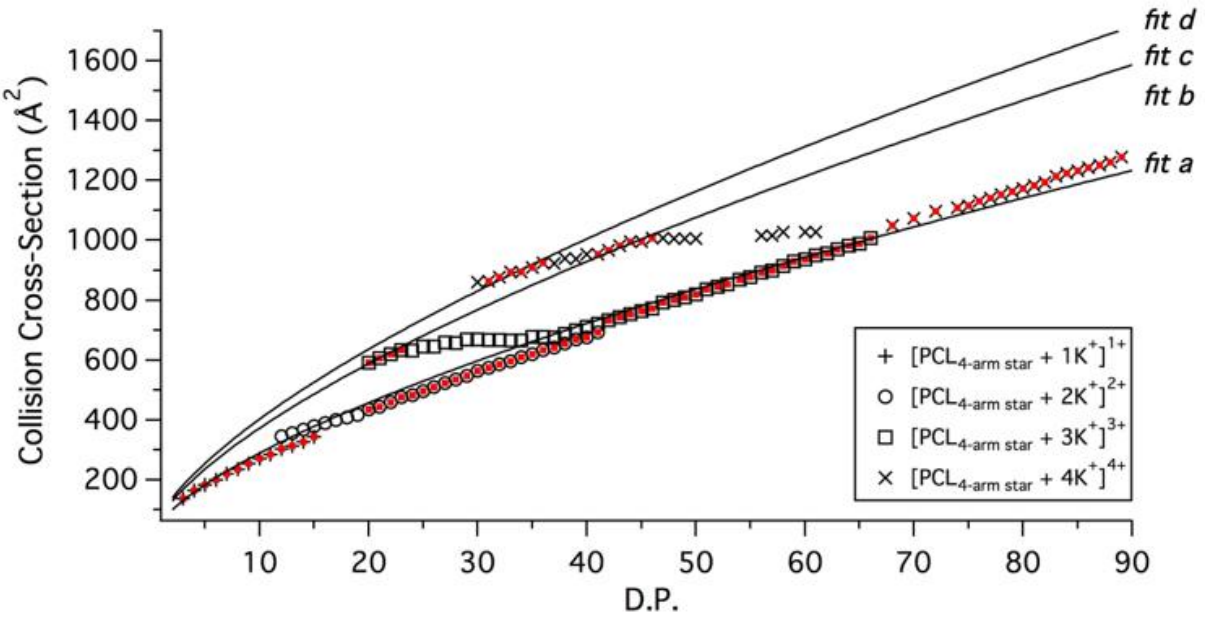

Figure SI15: Figure SI7 (CCS vs. DP of 4-arm star PCL) with highlighted data points (red dots) used for performing the data fits (*CCS = A.DP^{pow}, pow=0.66*).

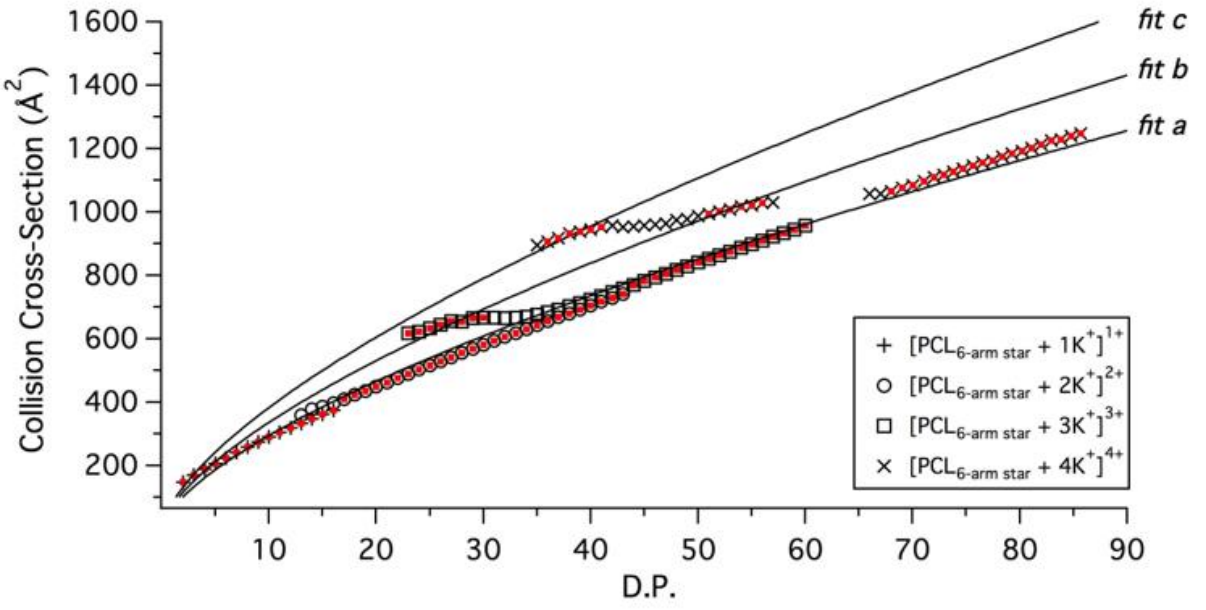

Figure SI16: Figure SI8 (CCS vs. DP of 6-arm star PCL) with highlighted data points (red dots) used for performing the data fits ($CCS = A.DP^{pow}$, *pow=0.66*).

Published in : Methods (2018), vol. 144, pp. 125–133
DOI: 10.1016/j.ymeth.2018.03.010
Status : Postprint (Author's version)

REFERENCES

[1] B. Clément, B. Grignard, L. Koole, C. Jérôme, P. Lecomte, Metal-free strategies for the synthesis of functional and well-defined polyphosphoesters, Macromolecules. 45 (2012) 4476–4486. doi:10.1021/ma3004339.

[2] R.C. Pratt, B.G.G. Lohmeijer, D.A. Long, P.N.P. Lundberg, A.P. Dove, H. Li, et al., Exploration, optimization, and application of supramolecular thiourea-amine catalysts for the synthesis of lactide (co)polymers, Macromolecules. 39 (2006) 7863–7871. doi:10.1021/ma061607o.

[3] B.G.G. Lohmeijer, R.C. Pratt, F. Leibfarth, J.W. Logan, D.A. Long, A.P. Dove, et al., Guanidine and amidine organocatalysts for ring-opening polymerization of cyclic esters, Macromolecules. 39 (2006) 8574–8583. doi:10.1021/ma0619381.

[4] A.P. Dove, R.C. Pratt, B.G.G. Lohmeijer, R.M. Waymouth, J.L. Hedrick, Thiourea-based bifunctional organocatalysis: Supramolecular recognition for living polymerization, J. Am. Chem. Soc. 127 (2005) 13798–13799. doi:10.1021/ja0543346.

[5] B.T. Ruotolo, J.L.P. Benesch, A.M. Sandercock, S.-J. Hyung, C. V Robinson, Ion mobility–mass spectrometry analysis of large protein complexes, Nat. Protoc. 3 (2008) 1139–1152. doi:10.1038/nprot.2008.78.

[6] A.E. Counterman, S.J. Valentine, C.A. Srebalus, S.C. Henderson, C.S. Hoaglund, D.E. Clemmer, High-order structure and dissociation of gaseous peptide aggregates that are hidden in mass spectra, J. Am. Soc. Mass Spectrom. 9 (1998) 743–759. doi:10.1016/S1044-0305(98)00052-X.

[7] M.F. Bush, I.D.G. Campuzano, C. V. Robinson, Ion mobility mass spectrometry of peptide ions: Effects of drift gas and calibration strategies, Anal. Chem. 84 (2012) 7124– 7130. doi:10.1021/ac3014498.

[8] S.J. Valentine, A.E. Counterman, D.E. Clemmer, Conformer-dependent proton-transfer reactions of ubiquitin ions, J. Am. Soc. Mass Spectrom. 8 (1997) 954–961. doi:10.1016/S1044-0305(97)00085-8.

[9] K.B. Shelimov, M.F. Jarrold, Vacuum : An Activation Barrier for Gas-Phase Protein Folding, J. Am. Chem. Soc. 119 (1997) 2987–2994.

[10] Y.L. Chen, B.A. Collings, D.J. Douglas, Collision cross sections of myoglobin and cytochrome c ions with Ne, Ar, and Kr, J. Am. Soc. Mass Spectrom. 8 (1997) 681–687. doi:10.1016/S1044-0305(97)00033-0.

[11] S.J. Valentine, J.G. Anderson, A.D. Ellington, D.E. Clemmer, Disulfide-Intact and Reduced Lysozyme in the Gas Phase: Conformations and Pathways of Folding and Unfolding, J. Phys. Chem. B. 101 (1997) 3891–3900. doi:10.1021/jp970217o.

[12] D. Morsa, T. Defize, D. Dehareng, C. Jérôme, E. De Pauw, Polymer topology revealed by ion mobility coupled with mass spectrometry, Anal. Chem. 86 (2014) 9693–9700. doi:10.1021/ac502246g.

Published in : Methods (2018), vol. 144, pp. 125–133
DOI: 10.1016/j.ymeth.2018.03.010
Status : Postprint (Author's version)

References

[1] J. Gidden, T. Wyttenbach, J.J. Batka, P. Weis, M.T. Bowers, Cationized by alkali ions: structures, energetics, and their effect on mass spectra and the matrixassisted laser desorption/ionization process, J. Am. Soc. Mass Spectrom. 305 (1999) 883–895, https://doi.org/10.1016/S1044-0305(99)00054-9.

[2] J. Gidden, M.T. Bowers, A.T. Jackson, J.H. Scrivens, Gas-phase conformations of cationized poly(styrene) oligomers, J. Am. Soc. Mass Spectrom. 13 (2002) 499– 505, https://doi.org/10.1016/S1044-0305(02)00367-7.

[3] J. Gidden, T. Wyttenbach, A.T. Jackson, J.H. Scrivens, M.T. Bowers, C.V. Ts, et al., Gas-phase conformations of synthetic polymers: poly (ethylene glycol), poly (propylene glycol), and poly (tetramethylene glycol), J. Am. Chem. Soc. 122 (2000) 4692–4699, https://doi.org/10.1021/JA993096+.

[4] D. Morsa, T. Defize, D. Dehareng, C. Jérôme, E. De Pauw, Polymer topology revealed by ion mobility coupled with mass spectrometry, Anal. Chem. 86 (2014) 9693–9700, https://doi.org/10.1021/ac502246g.

[5] G. von Helden, T. Wyttenbach, M.T. Bowers, Inclusion of a MALDI ion source in the ion chromatography technique: conformational information on polymer and biomolecular ions, Int. J. Mass Spectrom. Ion Process. 146–147 (1995) 349–364, https://doi.org/10.1016/0168-1176(95)04211-3.

[6] T. Wyttenbach, G. Von Helden, M.T. Bowers, Conformations of alkali ion cationized polyethers in the gas phase: polyethylene glycol and bis[(benzo-15-crown-5)-15-ylmethyl]pimelate, Int. J. Mass Spectrom. Ion Process. 165–166 (1997) 377–390, https://doi.org/10.1016/S0168-1176(97)00179-1.

[7] J. De Winter, V. Lemaur, R. Ballivian, F. Chirot, O. Coulembier, R. Antoine, et al., Size dependence of the folding of multiply charged sodium cationized polylactides revealed by ion mobility mass spectrometry and molecular modelling, Chem. Eur. J. 17 (2011) 9738–9745, https://doi.org/10.1002/ chem.201100383.

[8] S. Trimpin, M. Plasencia, D. Isailovic, D.E. Clemmer, Resolving oligomers from fully grown polymers with IMS-MS, Anal. Chem. 79 (2007) 7965–7974, https:// doi.org/10.1021/ac071575i.

[9] C. Larriba, J. Fernandez De La Mora, The gas phase structure of Coulombically stretched polyethylene glycol ions, J. Phys. Chem. B 116 (2012) 593–598, https://doi.org/10.1021/jp2092972.

[10] G. Von Helden, M.T. Hsu, N. Gotts, M.T. Bowers, Carbon cluster cations with up to 84 atoms: Structures, formation mechanism, and reactivity, J. Phys. Chem. 97 (1993) 8182–8192, https://doi.org/10.1021/j100133a011.

[11] A.E. Counterman, D.E. Clemmer, Gas phase polyalanine: assessment of i → i + 3 and i → i + 4 helical turns in [Alan + 4H]4+ (n = 29–49) ion, J. Phys. Chem. B 106 (2002) 12045–12051, https://doi.org/10.1021/jp021364b.

[12] A.E. Counterman, D.E. Clemmer, Compact → extended helix transitions of polyalanine in vacuo, J. Phys. Chem. B 107 (2003) 2111–2117, https://doi.org/ 10.1021/jp0213349.

[13] A.E. Counterman, D.E. Clemmer, Anhydrous polyproline helices and globules, J. Phys. Chem. B 108 (2004) 4885–4898, https://doi.org/10.1021/Jp036454a.

[14] C. Bleiholder, N.F. Dupuis, T. Wyttenbach, M.T. Bowers, Ion mobility–mass spectrometry reveals a conformational conversion from random assembly to b-sheet in amyloid fibril formation, Nat. Chem. 3 (2011) 172–177, https://doi.org/10.1038/nchem.945.

[15] S. Ude, J. Fernández De La Mora, B.A. Thomson, Charge-induced unfolding of multiply charged polyethylene glycol ions, J. Am. Chem. Soc. 126 (2004) 12184–12190, https://doi.org/10.1021/ja0381306.

[16] Q. Duez, T. Josse, V. Lemaur, F. Chirot, C.M. Choi, P. Dubois, et al., Correlation between the shape of the ion mobility signals and the stepwise folding process of polylactide ions, J. Mass Spectrom. 52 (2017) 133–138, https://doi.org/10.1002/jms.3915.

[17] J.R.N. Haler, J. Far, A. Aqil, J. Claereboudt, N. Tomczyk, K. Giles, et al., Multiple gas-phase conformations of a synthetic linear poly(acrylamide) polymer observed using ion mobility-mass spectrometry, J. Am. Soc. Mass Spectrom. 28 (2017) 2492–2499, https://doi.org/10.1007/s13361-017-1769-x.

Published in : Methods (2018), vol. 144, pp. 125–133
DOI: 10.1016/j.ymeth.2018.03.010
Status : Postprint (Author's version)

[18] A.E. Counterman, S.J. Valentine, C.A. Srebalus, S.C. Henderson, C.S. Hoaglund, D. E. Clemmer, High-order structure and dissociation of gaseous peptide aggregates that are hidden in mass spectra, J. Am. Soc. Mass Spectrom. 9 (1998) 743–759, https://doi.org/10.1016/S1044-0305(98)00052-X.

[19] C. Larriba, J.F. De La Mora, D.E. Clemmer, Electrospray ionization mechanisms for large polyethylene glycol chains studied through tandem ion mobility spectrometry, J. Am. Soc. Mass Spectrom. 25 (2014) 1332–1345, https://doi.org/10.1007/s13361-014-0885-0.

[20] J.N. Hoskins, S. Trimpin, S.M. Grayson, Architectural differentiation of linear and cyclic polymeric isomers by ion mobility spectrometry-mass spectrometry, Macromolecules. 44 (2011) 6915–6918, https://doi.org/10.1021/ma2012046.

[21] C.D. Foley, B. Zhang, A.M. Alb, S. Trimpin, S.M. Grayson, Use of Ion mobility spectrometry-mass spectrometry to elucidate architectural dispersity within star polymers, ACS Macro Lett. 4 (2015) 778–782, https://doi.org/10.1021/acsmacrolett.5b00299.

[22] K. Kim, J.W. Lee, T. Chang, H.I. Kim, Characterization of polylactides with different stereoregularity using electrospray ionization ion mobility mass spectrometry, J. Am. Soc. Mass Spectrom. 25 (2014) 1771–1779, https://doi.org/10.1007/s13361-014-0949-1.

[23] M.F. Mesleh, J.M. Hunter, A.A. Shvartsburg, G.C. Schatz, M.F. Jarrold, Structural information from ion mobility measurements: effects of the long-range potential, J. Phys. Chem. 100 (1996) 16082–16086, https://doi.org/10.1021/jp961623v.

[24] A.A. Shvartsburg, M.F. Jarrold, An exact hard-spheres scattering model for the mobilities of polyatomic ions, Chem. Phys. Lett. 261 (1996) 86–91, https://doi. org/10.1016/0009-2614(96)00941-4.

[25] C. Larriba, C.J. Hogan, Ion mobilities in diatomic gases: measurement versus prediction with non-specular scattering models, J. Phys. Chem. A. 117 (2013) 3887–3901, https://doi.org/10.1021/jp312432z.

[26] C. Larriba, C.J. Hogan, Free molecular collision cross section calculation methods for nanoparticles and complex ions with energy accommodation, J. Comput. Phys. 251 (2013) 344–436, https://doi.org/10.1016/j.jcp.2013.05.038.

[27] B. Clément, B. Grignard, L. Koole, C. Jérôme, P. Lecomte, Metal-free strategies for the synthesis of functional and well-defined polyphosphoesters, Macromolecules. 45 (2012) 4476–4486, https://doi.org/10.1021/ma3004339.

[28] B.T. Ruotolo, J.L.P. Benesch, A.M. Sandercock, S.-J. Hyung, C.V. Robinson, Ion mobility–mass spectrometry analysis of large protein complexes, Nat. Protoc. 3 (2008) 1139–1152, https://doi.org/10.1038/nprot.2008.78.

[29] M.F. Bush, I.D.G. Campuzano, C.V. Robinson, Ion mobility mass spectrometry of peptide ions: Effects of drift gas and calibration strategies, Anal. Chem. 84 (2012) 7124–7130, https://doi.org/10.1021/ac3014498.

[30] S.J. Valentine, A.E. Counterman, D.E. Clemmer, Conformer-dependent protontransfer reactions of ubiquitin ions, J. Am. Soc. Mass Spectrom. 8 (1997) 954– 961, https://doi.org/10.1016/S1044-0305(97)00085-8.

[31] K.B. Shelimov, M.F. Jarrold, Vacuum: an activation barrier for gas-phase protein folding, J. Am. Chem. Soc. 119 (1997) 2987–2994.

[32] Y.L. Chen, B.A. Collings, D.J. Douglas, Collision cross sections of myoglobin and cytochrome c ions with Ne, Ar, and Kr, J. Am. Soc. Mass Spectrom. 8 (1997) 681–687, https://doi.org/10.1016/S1044-0305 (97)00033-0.

[33] S.J. Valentine, J.G. Anderson, A.D. Ellington, D.E. Clemmer, Disulfide-intact and -reduced lysozyme in the gas phase: conformations and pathways of folding and unfolding, J. Phys. Chem. B. 101 (1997) 3891–3900, https://doi.org/10.1021/jp970217o.

[34] E.A. Mason, E.W. McDaniel, Transport properties of ions in gases, Wiley, New York, 1988. 10.1002/3527602852.

[35] E. Kendrick, A. Mass, Scale based on CH2 = 14.0000 for high resolution mass spectrometry of organic compounds, Anal. Chem. 35 (1963) 2146–2154, https://doi.org/10.1021/ac60206a048.

[36] S. Kokubo, P. Vana, Easy access to the characteristic ratio of polymers using ion-mobility mass spectrometry, Macromol. Chem. Phys. 218 (2017) 1600373, https://doi.org/10.1002/macp.201600373.

Published in : Methods (2018), vol. 144, pp. 125–133
DOI: 10.1016/j.ymeth.2018.03.010
Status : Postprint (Author's version)

[37] J.R.N. Haler, C. Kune, P. Massonnet, C. Comby-Zerbino, J. Jordens, M. Honing, et al., Comprehensive ion mobility calibration: poly(ethylene oxide) polymer calibrants and general strategies, Anal. Chem. 89 (2017) 12076–12086, https://doi.org/10.1021/acs.analchem.7b02564.

[38] J.R.N. Haler, P. Massonnet, F. Chirot, C. Kune, C. Comby-Zerbino, J. Jordens, et al., Comparison of different ion mobility setups using poly (ethylene oxide) PEO polymers: drift tube, TIMS, and T-wave, J. Am. Soc. Mass Spectrom. 29 (2017) 114–120, https://doi.org/10.1007/s13361-017-1822-9.

[39] P. Atkins, J. De Paula, Molecular reation dynamics, in: Atkins' Phys. Chem., 8th ed., Oxford University Press, 2006: pp. 869–908.

[40] A. Maißer, V. Premnath, A. Ghosh, T.A. Nguyen, M. Attoui, C.J. Hogan, Determination of gas phase protein ion densities via ion mobility analysis with charge reduction, Phys. Chem. Chem. Phys. 13 (2011) 21630, https://doi.org/10.1039/c1cp22127b.

[41] P. Massonnet, J.R.N. Haler, G. Upert, M. Degueldre, D. Morsa, N. Smargiasso, et al., Ion mobility-mass spectrometry as a tool for the structural characterization of peptides bearing intramolecular disulfide bond(s), J. Am. Soc. Mass Spectrom. 27 (2016) 1637–1646, https://doi.org/10.1007/s13361016-1443-8.

[42] J.C. May, C.R. Goodwin, J.A. McLean, Ion mobility-mass spectrometry strategies for untargeted systems, synthetic, and chemical biology, Curr. Opin. Biotechnol. 31 (2015) 117–121, https://doi.org/10.1016/j.copbio.2014.10.012.

[43] J.C. May, C.R. Goodwin, N.M. Lareau, K.L. Leaptrot, C.B. Morris, R.T. Kurulugama, et al., Conformational ordering of biomolecules in the gas phase: Nitrogen collision cross sections measured on a prototype high resolution drift tube ion mobility-mass spectrometer, Anal. Chem. 86 (2014) 2107–2116, https://doi. org/10.1021/ac4038448.